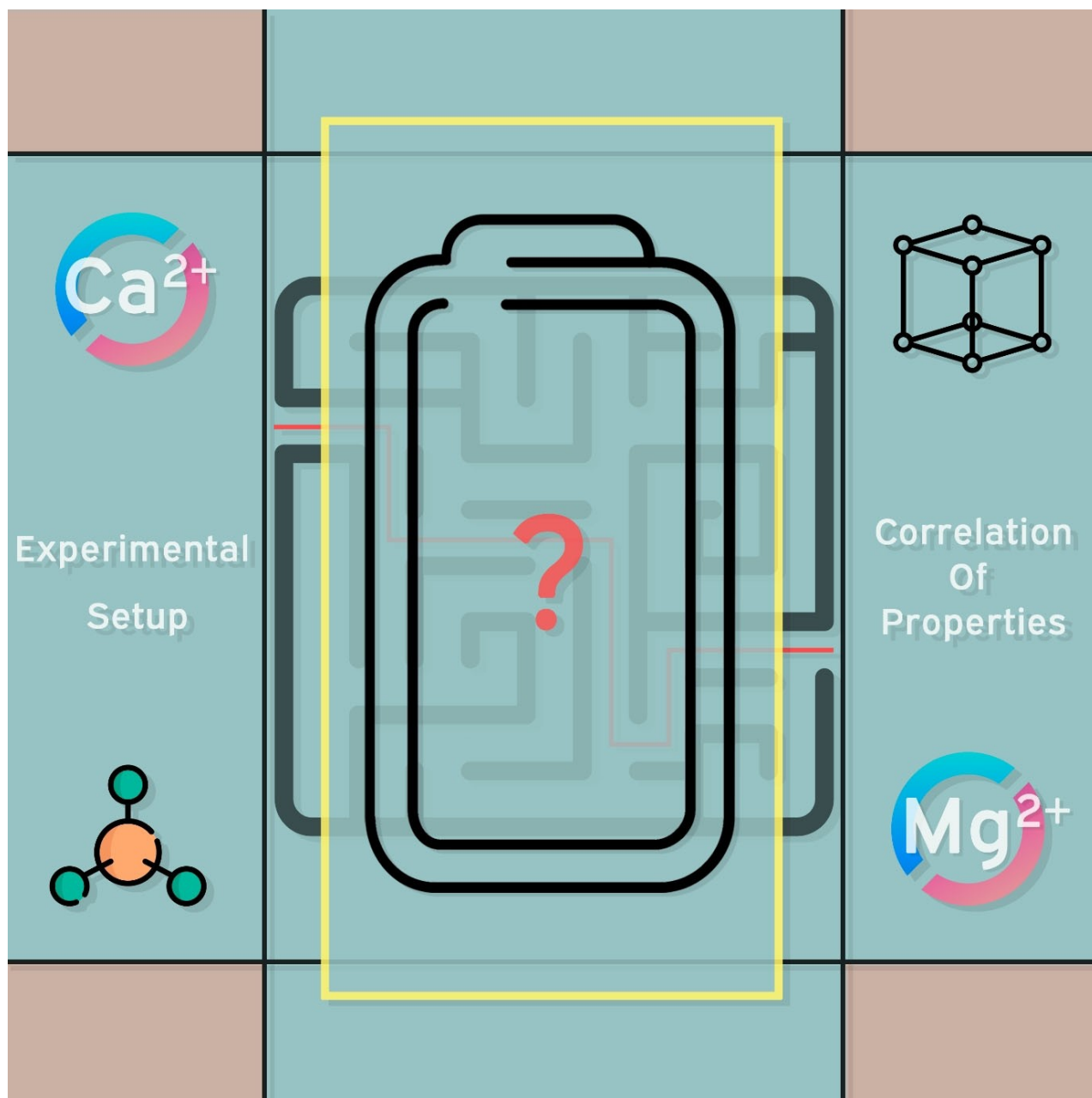


Special
Collection

Through the Maze of Multivalent-Ion Batteries: A Critical Review on the Status of the Research on Cathode Materials for Mg²⁺ and Ca²⁺ Ions Insertion

Fabio Maroni,^[a] Saustin Dongmo,^[a] Cornelius Gauckler,^[a] Mario Marinaro,^{*[a]} and Margret Wohlfahrt-Mehrens^[a, b]



This review aims to address the status of transition metal-based cathode materials for Mg^{2+} and Ca^{2+} -based multivalent-ion batteries on a critical standpoint, providing a comprehensive overview. Multivalent-based ions battery (MIB) technologies are among the most promising post-lithium electrochemical energy storage devices currently studied, but they still fall short in several aspects due to their early stage of research. In addition, difficult experimental conditions related to the electrolyte

systems and the cathode materials require an additional quote of care when performing experiments. In this review, a global approach is undertaken, from an introduction to electrolytes to the studied insertion parameters that allow a fast (de)insertion of multivalent ions. Then, the currently studied structural classes of cathode materials and a critical comment on data reporting, which are among the focal points of the actual state-of-the-art research, are thoroughly discussed.

1. Introduction

Envisioning a strategy to drive a long term transition to a greener economy, based on renewable energy sources, needs reliable secondary electrochemical energy storage systems to be developed.^[1] These systems need to deliver consistent performance in terms of safety, cost, discharge rate and environmental compatibility. Considering the current status of the energy storage market, the overly dominant, state-of-the-art and best performing technology is the so-called "rocking-chair" Lithium-ion battery (LIB),^[2] whose development started in the 70s, but only marketed in the early 90s by Sony.^[3]

LIBs are now largely widespread in every kind of portable device and transportation, from smartphones to Plug-in Hybrid (PHEV) and Battery powered electrical vehicles (BEV).^[4] The constant and only reliance on LIBs as the only marketed technology, poses several issues in terms of inhomogeneous worldwide distribution and raw materials supplies as well as toxic Cobalt-containing cathode materials.^[5] Moreover, the use of volatile and expensive organic electrolytes, and a non-less important recycling concern, growing on par with the increased market spread of this technology, which while on one hand can be addressed by the so-called "second-life" of LIBs, on the other hand still needs a decisive resolution.^[6]

One way to address the issues connected with LIBs, in order to find a viable alternative, are the several so-called "post-Li" chemistries that are currently under investigation. Historically, the development of non-Li related chemistries dates long ago, since the beginning of 20th century, but the advent of LIB research, shifted all the interest elsewhere. Among those, Sodium-Ion batteries (SIBs) have been the most researched and developed,^[7] also thanks to their partial similarity with LIBs, due to the single charge of the Na^+ cation, albeit having a much larger ion radius, similar electrolyte solutions and similar

investigated electrode materials. Despite this, full SIB cells show much lower specific energies than Li-ion batteries, mostly due to lower cell voltages and lower specific capacities of the electrode materials.

Multivalent-ions based chemistries (Ca^{2+} , Mg^{2+}), after few unsuccessful attempts to obtain satisfying electrochemical activity,^[8,9] found a new starting point in the early 2000s, with the proof-of-concept of a Rechargeable Magnesium Battery (RMB) from Aurbach et al.^[10] demonstrating the feasibility of such system for thousands of galvanostatic cycles using the so-called Chevrel-phase cathode.^[11] The battery prototype, despite having a low working potential (1.10 V vs Mg/Mg^{2+}) and gravimetric capacity ($\sim 100 \text{ mAh g}^{-1}$), ignited a burst of new interest in multivalent-ion based chemistries. Besides, Rechargeable Calcium Batteries (RCBs) obtained only recently the possibility of reversible plating/stripping at the metal anode,^[12,13] so the research in the field is still in its infancy.

On a chemical point of view, LIBs take great advantage from the lightness of Li, with the lowest mass among all the already cited metals, and the lowest redox potential, being -3.05 V vs. SHE. The low redox potential implies that the commonly used electrolyte solutions operate outside their electrochemical stability window, causing spontaneous decomposition reactions at the negative electrode, which passivate the anode surface, forming the so-called Solid Electrolyte Interphase (SEI).^[14] In addition to that, Li metal is known to undergo dendritic growth upon deposition, resulting in potential short-circuits which pose severe safety concerns.^[15]

Sodium metal has a higher redox potential with respect to Lithium (-2.71 V vs SHE), increased weight and larger ionic radius ($r_{Li^+} = 0.76 \text{ \AA}$ vs. $r_{Na^+} = 1.02 \text{ \AA}$). However, it is remarkably more abundant and cheaper than Lithium.^[16] The larger radius guarantees a less polarizing character, which can favor diffusion inside transition metal hosts and possibly an easier desolvation process at the interface. Despite these potentially good features and chemical similarities with Lithium, that allowed to easily obtaining stable electrolyte salts analogues (e.g. $LiPF_6$ to $NaPF_6$), the different ionic radii and different favored coordination environments ($CN=4$ for Li^+ and $CN=6$ for Na^+),^[17] cause a different behavior with known transition metal oxide hosts. In the case of sodium, this leads to very complicated crystal structure evolutions in most cases and in the end, the lack of a stable and suitable long lasting cathode material.

Crossing the fence to the multivalent-ion battery side, Magnesium (-2.37 V vs. SHE) and Calcium (-2.87 V vs. SHE) based chemistries are now receiving a good amount of interest

[a] Dr. F. Maroni, Dr. S. Dongmo, C. Gauckler, Dr. M. Marinaro,

Dr. M. Wohlfahrt-Mehrens

Zentrum Für Sonnenenergie Und Wasserstoff Forschung

Baden-Württemberg (ZSW)

Helmholtzstraße 8, 89081, Ulm

Germany

E-mail: mario.marinaro@zsw-bw.de

[b] Dr. M. Wohlfahrt-Mehrens

Helmholtz Institute Ulm (HIU) Electrochemical Energy Storage

Helmholtzstraße 11, 89081 Ulm

Germany

An invited contribution to a joint Special Collection between ChemElectroChem and Batteries & Supercaps dedicated to research Beyond Lithium-Ion Batteries.

from the research community.^[18] These alternative battery chemistries promise abundance, cheapness and increased volumetric capacity with respect to the established LIB technology- i.e. 2060 mAh⁻¹ for Li-metal, 3830 mAh⁻¹ for Mg-metal and 2073 mAh⁻¹ for Ca metal which can partially compensate for the increased weight. Following the so-called “diagonal relationship” on the periodic table of elements, Magnesium and Calcium should possess similar chemical features with respect to their Alkali metal homologues, Lithium and Sodium, respectively. In fact the respective ionic radii are 0.72 Å for Mg²⁺ (vs. 0.76 Å for Li⁺) and 1 Å for Ca²⁺ (vs. 1.02 Å for Na⁺), electronegativity is 1.31 for Mg (vs. 0.98 for Li) and 1 for Ca (vs. 0.93 for Na) (See Table 1). Just basing the argument on those properties, one could think that Mg and Ca chemistries would be comparable to the “traditional” Li and Na, but that is not the case, as widely demonstrated by literature data. Considering the doubled charge density and the different preferred coordination environments, with the coordination numbers for Mg²⁺ and Ca²⁺ being 6 and ranging from 6 to 8



Dr. Fabio Maroni received his Ph.D. from the University of Camerino in 2015, working on new materials for Li-ion batteries under the supervision of Prof. Dr. Francesco Nobili. After two years of postdoc following up the Ph.D. work, he moved to the University Of Chieti-Pescara “G. D’Annunzio”, to join Prof. Fausto Croce’s group, working on all-solid-state lithium batteries. In 2020, he moved to the Zentrum für Sonnenenergie-und Wasserstoff-Forschung Baden-Württemberg (ZSW) to work on new post-lithium chemistries, within the DFG funded POLIS Cluster of Excellence, with Team Leader Dr. Mario Marinaro, in the group of Dr. Margret Wohlfahrt-Mehrens.



Dr. Saustin Dongmo received his Ph.D. in chemistry from the University of Oldenburg in Germany in 2017. Then he joined the research group of Prof. Jürgen Janek as a postdoctoral researcher at the Justus-Liebig University Giessen working on secondary zinc-air batteries with the junior group leader Dr.-Ing. Daniel Schröder. Currently, he is working at the Zentrum für Sonnenenergie-und Wasserstoff-Forschung Baden-Württemberg (ZSW) on post-lithium battery technologies, within the POLIS Cluster of Excellence with Team Leader Dr. Marinaro in the group of Dr. Margret Wohlfahrt-Mehrens.



Cornelius Julian Gauckler received his B.Sc. in the department of Prof. Dr. Rolf Jürgen Behm of Surface Chemistry and Catalysis at the Ulm University in 2017. Afterwards, he completed his M.Sc. at the Zentrum für Sonnenenergie- und Wasserstoff-Forschung Baden-Württemberg (ZSW) in Ulm in 2019. He is currently a Ph.D. student at ZSW, working on new post-lithium systems within the DFG funded POLIS Cluster of Excellence, with Team Leader Dr. Mario Marinaro, in the group of Dr. Margret Wohlfahrt-Mehrens.

respectively,^[19] Mg and Ca were found to be in a class of their own when tested as potential battery chemistries. In general, multivalent-ion battery chemistry development, face a series of serious hurdles, which are not easy to overcome, and require the full attention of the research community.

Magnesium battery research is still closely tied in the search for a simple, reproducible and widely stable electrolyte system, compatible with the metal anode, but able to employ high voltage cathode materials to increase the energy. Historically, from the Grignard reagents studied in early times,^[9] to the organohaloaluminate systems and their evolutions studied by Gregory,^[22] to the MACC (MgCl₂–AlCl₃) electrolyte by Aurbach et al.^[23] to the more recent HMDS-derived electrolytes^[24] boron-based electrolytes,^[25] and organometallic-based species,^[26] despite proceeding towards the objective with good improvements, still failed it. In this regard, the use of limitedly stable and volatile ethereal solvents like THF and the unique and very complicated organometallic nature of Mg²⁺ solution chemistry, not comparable with any other known system until now, is still



Dr. Mario Marinaro received his Ph.D. from the University of Camerino (Italy) working on negative electrodes for Li-ion batteries under the supervision of Prof. Roberto Marassi. He then moved to the ZSW (Zentrum für Sonnenenergie- und Wasserstoff-Forschung Baden-Württemberg) as post-doctoral research associate focusing on metal-air batteries and alloy-type anodes for Li-ion batteries. In 2017, Dr. Marinaro was appointed Team Leader at ZSW in the group of Dr. Margret Wohlfahrt-Mehrens. In 2020, he also joined the Post Lithium Storage Cluster of Excellence (POLIS) as Key Researcher & Group Coordinator and became Associate Fellow in 2021. His main research interests focus on advanced lithium- and post-lithium battery technologies.



Dr. Margret Wohlfahrt-Mehrens is head of the Department of Accumulators Materials Research at the ZSW (Zentrum für Sonnenenergie- und Wasserstoff-Forschung, Baden-Württemberg) in Ulm, Germany. She studied Chemistry at the University of Bonn and received her Ph.D. in Chemistry from the University Witten/Herdecke in 1989. She has been working in the field of electrochemical energy storage systems (mainly in the field of lithium-ion batteries) at ZSW since 1990. She is member of the board of directors of the Helmholtz Institute Ulm (HIU) and leader of a research unit in the Post Lithium Storage Cluster of Excellence (POLIS).

Table 1. Comparison of properties of Li, Na, Mg, and Ca.^[20,21]

Element	E vs. SHE [V]	Ionic radius [Å]	Volumetric capacity [mAh ml ⁻¹]	Specific capacity [mAh g ⁻¹]	Polarization strength [10 ⁴ pm ⁻²]	Coordination preference
Li	-3.04	0.76	2026	3861	2.16	octahedral and tetrahedral
Na	-2.71	1.02	1128	1165	1.11	octahedral and prismatic
Mg	-2.37	0.72	3833	2202	4.73	octahedral
Ca	-2.87	1	2073	1337	/	octahedral

an added hurdle faced every day. Simple electrolyte solutions prepared by dissolving a single salt in an organic solvent (acetonitrile, organic carbonates), usually have wide electrochemical stability windows and do not suffer from complex solution chemistry, but are well known as incompatible with the Mg metal anode.^[27] This leads to decomposition reactions and passivation of the metal anode, which differently from the LIB case, is not a ionically conductive layer,^[28] thus completely blocking any kind of electrochemical activity. Alternative anode material research is under way^[29] but it's still a long way to go.

On the other hand, research activities on RCBs, started to emerge in the 60s,^[8] but only in the systematic studies of Aurbach et al.,^[27] several solvents and salts were tested in order to obtain useful information about possible Ca stripping/plating, ending in the hypothesis that also the passivation layer formed on top of the metal is non ionically conductive, thus stopping any kind of possible electrochemical activity. Only recently, with two breakthroughs, a reversible plating/stripping at the calcium metal surface was obtained, respectively with $\text{Ca}(\text{BH}_4)_2/\text{THF}$ at room temperature and $\text{Ca}(\text{BF}_4)_2/\text{EC:PC}$ at 100 °C.^[12,13,30,31] Alternative anode materials have just been little explored, with alloying Sn-based anodes showing promising capabilities and preliminary evaluations on Si-based materials.^[32]

Theoretical calculation tools are becoming more and more used to help in the process^[33] of screening and selecting materials, which has been very useful in the search for suitable cathode materials, historically being the limiting side for every modern electrochemical energy storage device. Traditional materials like TiS_2 ,^[34] V_2O_5 ,^[35] MnO_2 ,^[36] spinels,^[37] Chevrel and perovskite phases^[38,39] and Prussian Blue Analogues (PBAs)^[40] have been probed for Mg^{2+} and Ca^{2+} insertion, either electrochemically and/or theoretically (DFT calculations), but until now, results haven't been returning quite a clear picture of the situation.

In this review, a global approach will be undertaken to take a critical look at the state of the art of positive material research for Mg and Ca-based batteries. Starting from an overview of

the used electrolyte systems and examining the parameters that could possibly influence an efficient (de)insertion of multivalent ions inside known host materials, the focus will be on individual classes of transition metal hosts with different crystal structures. In addition, to ensure a consistent discussion about the reviewed data, a comment about data reporting and suggestion is added.

2. Electrolyte Systems for $\text{Mg}^{2+}/\text{Ca}^{2+}$ Insertion

The electrolyte is an ion-transport environment placed between the cathode and the anode which should have the following characteristics: i) high ionic conductivity and no electronic conductivity; ii) wide electrochemical stability window, iii) good thermal stability, iv) low volatility and low flammability v) non-corrosivity.^[41] Several review papers reported the historical development of electrolytes for Mg and Ca batteries, although mostly dedicated to the anode side.^[41–44] Unfortunately, electrolytes capable of enabling an efficient metal stripping/plating are often plagued by a low anodic stability. Therefore, only a few of the existing cathode materials, mainly working at low potentials (i.e. Chevrel phases) are able to work in synergy with an anode-compatible electrolytes.^[45]

The available literature on cathode materials for Ca^{2+} or Mg^{2+} insertion/intercalation shows almost the same type of salts and solvents used with LIBs and SIBs (See Figure 1). Most of those do not enable the stripping/plating of alkali earth metals but have good stability toward oxidation. Moreover, often there is not a clear indication why a specific electrolyte formulation is selected or, at least, these reasons are not fully elucidated. As an example, V_2O_5 or MoO_3 electrodes able to insert different variety of cations, have been used with different salts and solvent to insert Mg^{2+} or Ca^{2+} . Acetonitrile (ACN) and propylene carbonate (PC) are often used with $\text{Mg}(\text{TFSI})_2$, $\text{Mg}(\text{ClO}_4)_2$, $\text{Ca}(\text{TFSI})_2$, or $\text{Ca}(\text{ClO}_4)_2$.

Recently developed halide-free or non-corrosive $\text{Mg}(\text{CB}_{11}\text{H}_{12})_2/\text{tetraglyme}$ (TG) and $\text{Mg}[\text{B}(\text{hfip})_4]_2/1,2\text{-dimeth-$

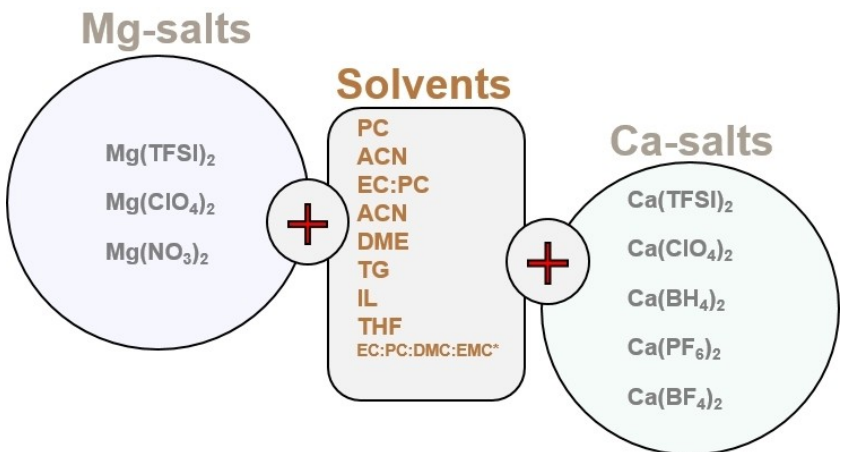


Figure 1. Overview of solvents and salts used frequently to investigate the new cathode materials for Mg and Ca insertion (*the salts commonly used to plate and strip are excluded*).^[43,44] *: only used in calcium battery.

oxyethane (DME) electrolytes, represent some exceptions owing to their high anodic stability, 4.00 V and 4.30 V vs Mg/Mg^{2+} , respectively, on a stainless steel^[31,46,47] current collector. Intercalation of Mg^{2+} cations was investigated in a full Mg-ion battery cell using $NaV_{1.25}Ti_{0.75}O_4$ as cathode material, $Mg(CB_{11}H_{12})_2/TG$ electrolyte and a Mg metal anode.^[48] A study on Mg^{2+} intercalation kinetics was conducted using $Mg[B(hfip)_4]_2/DME$ electrolyte and MoS_2 cathode.^[49] However, due to its high viscosity and the strong coordination of the TG solvent, the $Mg(CB_{11}H_{12})_2/TG$ system hinders the ionic motion and leads to slower kinetics at the electrolyte-electrode interface, thus making it unfavorable for high power-density applications. Furthermore, synthesis of the carborane anion ($CB_{11}H_{12}^-$)-containing precursors requires multistep reactions, in addition to being costly and commercially limited.^[50] Finally, despite its high anodic stability, $Mg[B(hfip)_4]_2/DME$ performance seems to be highly influenced by the quality of the $Mg(BH_4)_2$ precursor salt used for its synthesis.^[51]

Notwithstanding the good amount of research data that has been published in these last few years, research on cathode materials and electrolytes for multivalent battery cells is still in an early stage. The lack of a “reference” high-potential cathode material for both Mg^{2+} and Ca^{2+} insertion, as well as a widely used standard electrolyte formulation is still an issue to be solved by the scientific community (See Table 2). Thus a systematic investigation on the impact of electrolyte formulations should be encouraged and later benchmarked. Moreover, it is worth noting that the lack of reliable electrochemical cell setup/configuration, which will be later addressed in this review, also hinders the interpretation of the published results.

3. Factors Affecting Mg-Ion and Ca-Ion Insertion

Among the fundamental but yet not clearly answered questions in multivalent battery materials, there is a clear and

unambiguous characterization of the various parameters that can influence the efficient and reversible insertion of divalent cations into a host.

While, on the one hand, Mg^{2+} and Ca^{2+} share some similarities due to their divalent nature, their different cation radius, i.e. 0.72 Å for Mg^{2+} and 1 Å for Ca^{2+} , and consequently their different charge density, has some consequences, first of all in the development of viable electrolytes.

The insertion process of a metal ion in a host structure, from the bulk of the electrolyte to its suitable crystallographic site, can be seen as a series of consecutive steps and/or interfaces. Many parameters play a role within the ion journey into the host. Therefore, a careful consideration of such parameters is of primary importance in order to avoid misguidance and wrong interpretations and for the benefit of the battery community.

The first step, in the insertion process, can be found at the electrode-electrolyte interface. Historically, electrolyte investigations for Mg^{2+} and Ca^{2+} secondary batteries, had a quite different evolution, keeping in mind the fact that while on the one hand Mg chemistry had generated a remarkable research interest which led to the already mentioned proof-of-concept by Aurbach et al. in 2000,^[10] on the other hand, the interest on Ca^{2+} secondary batteries rose only in recent years.^[70]

Magnesium electrolytes are characterized by a quite unique variety of salts, solvents and reported concentrations. In addition to that, the lack of established investigation protocols about electrode-electrolyte interfaces makes difficult to uniquely identify and explain desolvation mechanisms, closely related to the hard Lewis acid nature of the Mg^{2+} . Moreover, electrolyte solutions able to reach higher potentials, at which insertion cathodes work (e.g. $Mg(ClO_4)_2/ACN$), are often not compatible with Mg metal anodes, with only few already mentioned exceptions.

Instead, most Ca electrolytes, due to the softer nature of the Ca^{2+} cation, are prepared by means of a simpler and more widespread approach, using readily available solvents/salts such as those used in Na-ion or Li-ion batteries. Furthermore,

Table 2. Selected cathode materials and electrolytes

Structural category	Material	Electrolyte	Cell Setup	Electrodes ^[a]	Ref.
Layered	MoO _{2.8} F _{0.2}	Mg(TFSI) ₂ 0.2 M/Propylene carbonate	2 electrode cell (CR2032)	Carbon CE	[51]
	V ₂ O ₅ ·nH ₂ O@rGO	Mg(TFSI) ₂ 0.5 M/Acetonitrile (ACN)	3 electrode cell	Activated carbon CE/QRE	[52]
	V ₂ O ₅	Ca(ClO ₄) ₂ 0.4 M/Propylene carbonate (PC)	3 electrode cell	Activated carbon CE/Ag wire QRE	[53]
	NaV ₃ O ₈	Mg(ClO ₄) ₂ 0.5 M/ACN APC/MACC (CR2016)	3 electrode cell 2 electrode cell (CR2016)	Activated carbon CE/QRE Mg CE (CR2016)	[54]
	NH ₄ V ₄ O ₁₀	Mg(ClO ₄) ₂ 0.5 M/ACN	2 electrode Cell (homemade cell)	Activated carbon CE	[55]
	α-MoO ₃ thin film	Mg(TFSI) ₂ 0.1 M/ACN Mg(ClO ₄) ₂ 0.5 M/ACN	3 electrode Ag-filled sealed cell	Activated carbon cloth CE/QRE(on Pt wire)	[56]
	α-MoO ₃	Ca(TFSI) ₂ 0.5 M/1,2 Dimethoxyethane (DME) Ca(TFSI) ₂ 0.1 M/ACN	3 electrode cell 2 electrode cell	Ca metal CE/QRE Activated carbon CE (2 electrode cell)	[57]
	TiS ₂	Mg(ClO ₄) ₂ 1 M/ACN	2 electrode cell	Mg foil CE	[58]
	VOPO ₄	Mg(ClO ₄) ₂ 0.1 M/PC Mg(ClO ₄) ₂ ·6H ₂ O 0.1 M/PC	3 electrode cell	Carbon CE/Ag/AgCl QRE	[59]
Polyanion (Silicate)	FeSiO ₄	Mg(TFSI) ₂ 0.5 M/ACN	3 electrode cell	Mg ribbon CE/Ag wire QRE in 0.01 M AgNO ₃ + 0.1 M Mg(TFSI) ₂ in ACN	[60]
Polyanion (NASICON)	Mg _{0.5} Ti ₂ (PO ₄) ₃	Mg(TFSI) ₂ 0.1 M/PC	3 electrode glass cell	Mg ribbon CE/Ag wire in 0.1 M Ag(ClO ₄) ₂ /PC	[61]
Spinel	Ca _x NaV ₂ (PO ₄) ₃	Ca(TFSI) ₂ 1 M/CAN (desodiation) Ca(TFSI) ₂ 0.5 M/Diglyme (galvanostatic cycling)	2 electrode cell	Activated carbon CE	[62]
	MgMn ₂ O ₄	Mg(ClO ₄) ₂ 0.5/ACN	2 electrode cell (CR2032)	Activated carbon CE	[63]
	MgCo ₂ O ₄	Mg(ClO ₄) ₂ 1 M/ACN	2 electrode cell	Mg Metal CE/QRE	[64]
	MgMn ₂ O ₄	Mg(ClO ₄) ₂ 0.5 M/EC:DEC (50:50)	3 electrode cell	V ₂ O ₅ CE/Pt QRE	[65]
Prussian Blue Analog (PBA)	Ca _{0.5} Co ₂ O ₄	Ca(ClO ₄) ₂ ·4H ₂ O 1 M/ACN	2 electrode cell 3 electrode cell	V ₂ O ₅ CE/Ag/AgCl QRE (3 electrode cell)	[66]
	KNiFe(CN) ₆	Ca(TFSI) ₂ 0.5 M/ACN	3 electrode cell	Activated carbon CE/Ag QRE	[67]
	Na _{0.2} MnFe(CN) ₆	Ca(PF ₆) ₂ 0.2 M/EC:PC (3:7)	2 electrode cell 3 electrode cell	Activated carbon CE(2,3 electrode cell)/Ca metal(3 electrode cell)	[68]
Fluoro-Phosphate	NaFePO ₄ F	Ca(PF ₆) ₂ 0.2 M/EC:PC (3:7)	2 electrode cell (coin cell) 3 electrode cell	Carbon CE/Ca metal QRE	[69]

[a] CE: counter electrode, QRE: quasi reference electrode.

while the lower charge/radius ratio could make easier the desolvation process at the interface, at the same time the formation of a passivation layer on Ca-metal surface with a low-to-none Ca²⁺ ion mobility made difficult the room temperature plating/stripping until 2019,^[12,13] thus also limiting studies on Ca metal based full cells.

Shedding light on (de)solvation processes at the electrode/electrolyte interface is a notoriously hard task, and multivalent batteries make no exception. In this regard, only few studies are available in literature, making use of model compounds. Attias^[72] reported a comprehensive study about the solvent influence on charge/transfer kinetics at the electrode/electrolyte interface of a V₂O₅ insertion material. The authors considered parameters such as solvent co-intercalation, (de)solvation interactions, and possible film formation on the cathode material. The electrochemical investigations were carried-out in a three-electrode cell setup, using Activated Carbon (AC) as quasi-reference (QRE) and counter electrode (CE). The reference electrolyte solution was Mg(ClO₄)₂ in Acetonitrile (ACN), while dimethoxyethane (DME) was added to investigated its influence on the interface. By combining spectroscopic and electrochemical techniques (GITT, XPS and Raman) the authors were able to eliminate the possibility of a

negative influence of DME in solid-state diffusion processes and the possible formation of a surface film on the cathode, which could negatively impact the electrochemical performances. In the end, the negative effect of DME on the charge-transfer kinetics was identified in the formation of more stable ion solvates between DME-Mg²⁺ than ACN-Mg²⁺, determining an important result, since ether-based solvents are by far the most common solvent category in Mg-battery research. Solvent effects can play a fundamental role in the actual feasibility of multivalent-ions intercalation inside transition metal hosts, and more studies are needed to understand and tune those properties.

In terms of structural features, a good cation mobility within the cathode hosts is of paramount importance to obtain a reversible insertion at sufficiently high current densities to enable feasible battery prototypes. Due to their multivalent nature, Mg²⁺ and Ca²⁺ cations are expected to have increased interactions with the host and a reduced mobility, thus requiring in-depth investigations and careful structural screening to face this challenging hurdle, in the development of new and already known insertion materials for multivalent cations.

While for the well-established Li technology there is plenty of available data^[73] and the upcoming Na-ion batteries are also

taking advantage from an extensive research effort,^[74] multivalent insertion materials lack systematic spectroscopic investigations on insertion parameters and fundamental understanding of ion migration.

Aurbach and co-workers at Bar-Ilan University, in their pioneering work on Mg-batteries also reported a highly cited study in 2009^[75] in which the authors reviewed possible parameters influencing solid state diffusion in cathode materials for Mg-batteries, making a parallelism between Li⁺ and Mg²⁺ cations in M_xCoO₂ as model layered insertion material. Among them, the most important ones were identified as the multi-ion interactions and coordination environment, regarding the ion hopping processes inside cathode host frameworks, and charge redistribution, by variation of the oxidation state of the host transition metal cations. Excluding size as possible factor of slower diffusion for Mg²⁺ cations, the authors find as source of high cationic repulsion, the very short distance of 2 Å between the inserted cation and a Co atom in the intermediate tetrahedral used as transport during diffusion, also taking into account the 2+ charge of Mg with respect to Li⁺ cations. For this reason, a crystal structure in which a different transition metal cation distribution shows lower cation repulsions, like the spinel structure, is suggested as potential candidate for faster Mg-cation diffusion. Following that, the possibility of intercalating ions also in low-potential barrier tetrahedral sites (not used only as intermediate diffusion step) in spinels, accounts for this favorable perspective. Concerning charge redistribution, compensating the insertion of a 2+ charge cation, introduces an additional hurdle, since the severe oxidation state variation of a transition metal cation could induce mechanical stress on the crystal structure due to cation volume variation. In addition, the "hard" oxygen atom framework, is usually hardly polarizable. In any case, the deep

relationship between the inserted cation and the crystal structure of the host material is a fundamental point to be investigated.

Recently, theoretical studies and simulations by means of first principle DFT and NEB^[76] (Nudged Elastic Band) calculations, are becoming more and more important to speed up the process (See Table 3). Rong et al.,^[77] (See Figure 2) reported in 2015 a detailed theoretical study on energy migration barriers inside model host materials such as spinel Mn₂O₄, olivine FePO₄, layered NiO₂ and orthorhombic δ-V₂O₅, comparing monovalent Li⁺ with divalent Mg²⁺, Zn²⁺ and Ca²⁺ cations. The study points out that for these multivalent cations, there is no unique structure "to fit them all", and each cation can have a better (or worse) mobility, depending on the host structure. To have a better picture, the authors suggest to pair diffusion topology data of each cation with its preferred crystal insertion site. The authors estimated an energy migration barrier threshold (E_m) of ~525 meV for micron sized particles and ~650 meV for nano-sized particles, which despite being higher than Li⁺ barriers, should still allow for insertion/deinsertion processes. Calculations showed that depending on the cation and the structure, close-to-threshold barriers could be predicted for multivalent cations, e.g. Mg²⁺ in FePO₄ and Ca²⁺ in Mn₂O₄ and FePO₄. The migration energies have been then elucidated in terms of interactions between the multivalent cations and the anion coordination environment, i.e. taking into consideration the close-packed oxygen lattices of the model materials, and relating it to the possible migration path. In the chosen model compounds, tetrahedral and octahedral sites share a three-coordinated oxygen face. While the authors suggest that a direct migration between equivalent sites, e.g. octahedral → octahedral, is unfavored due to increased repulsion, a migration through an intermediate site of different coordination may

Table 3. Mg insertion compounds with assigned properties calculated by ab initio methods. The mobility barriers refer to the minimum activation barrier for an Mg²⁺ ion to traverse the entire compound unit cell. An activation barrier is defined as the difference in energy between two distinct Mg crystallographic sites and is computed by elastic band calculations.^[71]

Cathode material	Structural type	Migration barrier ^[a] [meV]	Average Voltage (vs. Mg/Mg ²⁺) [V]
FeCl ₃	Layered	619	2.34 (1e ⁻)
V ₂ (PO ₄) ₃	Polyanion	536	2.63 (3e ⁻)
Cr ₂ S ₄	Spinel	553	1.67 (2e ⁻)
Mn ₂ O ₄	Spinel	575	2.90 (2e ⁻)
CrS ₂	Layered	788	1.51 (2e ⁻)
FePO ₄ Olivine	Polyanion	608	2.66 (1e ⁻)
Ni ₂ O ₄	Spinel	626	3.52 (2e ⁻)
CrMo(PO ₄) ₃	Polyanion	591	2.42 (3e ⁻)
CoO ₂	Layered	674	3.18 (0.5e ⁻)
Mo ₂ (PO ₄) ₃	Polyanion	844	2.21 (3e ⁻)
MoPO ₄	Polyanion	853	2.16 (2e ⁻)
(CoMn)O ₄	Spinel	938	2.54 (2e ⁻)
TiP ₂ O ₇	Polyanion	449	0.61 (1e ⁻)
VS ₂ Spinel	VS ₂ Spinel	497	0.94 (2e ⁻)
V ₂ O ₄ Spinel	V ₂ O ₄ Spinel	504	2.25 (2e ⁻)
TiO ₂ Anatase	Anatase	547	0.67 (1e ⁻)
Alpha-VOPO ₄	Polyanion	548	2.37 (2e ⁻)
V ₁₈ O ₄₄	Pseudo-layered	156	2.37 (12e ⁻)
Beta-VOPO ₄	Pseudo-layered	774	2.58 (2e ⁻)
FeOCl	Layered	389	1.54 (1e ⁻)
V ₂ O ₅	Pseudo-layered	545	2.58 (2e ⁻)
V ₂ O ₅ (Common Ground State)	Pseudo-layered	564	2.43 (2e ⁻)

[a] By *ab initio* methods.

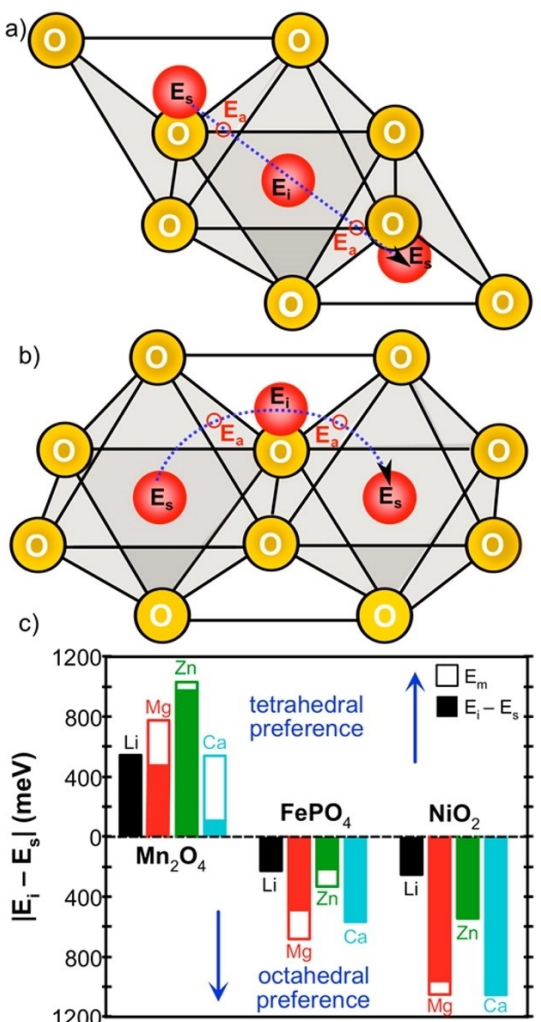


Figure 2. Low-energy ion migration paths in close-packed oxides adopt either a *a*) *tet*→*oct*→*tet* or *b*) *oct*→*tet*→*oct* diffusion topologies: beginning in the stable insertion sites (E_s), crossing through a three-coordinated oxygen face (E_a) into the intermediate site (E_i), and finally migrating to the next stable site through a symmetric path. Comparing the *c*) site energy difference $|E_i - E_s|$ between *tet* and *oct* sites (solid bars) to the migration barriers E_m (hollow bars) along the diffusion path for Li^+ , Mg^{2+} , Zn^{2+} , and Ca^{2+} in spinel Mn_2O_4 , olivine FePO_4 , and layered NiO_2 reveals the underlying influence of each intercalant's anion coordination preference on the migration barrier. Reprinted from Ref. [77] with permission. Copyright (2015) American Chemical Society.

have a lower energy barrier, depending on the favored coordination environment of each multivalent cation. As reported in literature, while Li^+ is often found in tetrahedral coordination environments Mg^{2+} is often found in six-fold coordination environments and Ca^{2+} is mostly eight-coordinated. For this reason, the insertion process of a multivalent cation in a host material characterized by sites with the favored coordination environment, could lead to a stable structure with very high migration barriers, as Mg^{2+} in olivine and layered structures mainly characterized by the presence of octahedral sites.

In a recent report Mao et al.,^[78] (See Figure 3) combined theoretical DFT calculations, X-ray diffraction (XRD), energy dispersive spectroscopy (EDS) and electrochemical techniques

to investigate Mg^{2+} insertion kinetics into selected layered compounds, trying to rationalize materials design principles from the anionic framework point of view. A series of MX_2 materials ($\text{M}=\text{Ti}, \text{V}; \text{X}=\text{O}, \text{S}, \text{Se}$) with a $\text{P}3\text{m}1$ structure were selected as models and screened via DFT. Based on their thermodynamic stability, TiS_2 , VS_2 , TiSe_2 and VSe_2 were found to be the most suitable model compounds. After synthesis, the three compounds were structurally and morphologically characterized, via XRD and SEM confirming the $\text{P}3\text{m}1$ structure and a comparable particle size. Preliminary electrochemical characterization was conducted in a 2032 coin-cell setup using the APC electrolyte, by means of cyclic voltammetry (CV) and galvanostatic cycling (GC). The Mg^{2+} insertion process was investigated and confirmed using EDS spectroscopy and ex-situ XRD of samples discharged at different potential values. Kinetic properties of the chosen materials were examined via galvanostatic intermittent titration technique (GITT), electrochemical impedance spectroscopy (EIS) and CV, revealing a diffusion-controlled insertion process with lower overpotentials and several orders of magnitude higher estimated diffusion coefficients for the selenide materials. These results were then used to investigate these differences in diffusive behaviors, in a second round of calculations using the NEB theory.

The migration barriers were calculated by considering a diffusion path in which the Mg^{2+} cation diffuses to equivalently stable sites (octahedral for MS_2 and MSe_2 ; tetrahedral for MO_2) through an intermediate differently coordinated site (tetrahedral for MS_2 and MSe_2 ; octahedral for MO_2), depending on the chosen model compound. The diffusion path is similar to that reported by Rong et al. Energy barrier values were above 1 eV for VO_2 , while 593 meV for VS_2 and a lower value of 349 meV for VSe_2 . The authors correlated these barriers with the decreasingly electronegative nature of the anions ($\text{Se}^{2-} > \text{S}^{2-} > \text{O}^{2-}$). These considerations about diffusion paths were then coupled with an extensive discussion about the deformability of the electron clouds, due to the interactions with the diffusing Mg^{2+} cations, indicating as positive a less ionic nature of the anionic framework bonds. The authors generalized these investigations among layered MX_2 compounds, into three criteria that can influence the cation mobility and can be used to improve it: (i) larger diffusion channels due to bigger anions (ii) weaker interactions between the anionic framework and the cation exploiting a more deformable electronic cloud (iii) higher electronic conductivity. Though all these considerations were developed for trigonal layered materials, they were suggested to be applicable also to monoclinic ($\text{P}21\text{m}$) and triclinic ($\text{P}1$) materials.

4. Magnesium Cathode Materials

It must be recognized that the search for new anode materials for Mg-batteries, compatible with conventional electrolytes such as $\text{Mg}(\text{ClO}_4)_2$ or $\text{Mg}(\text{TFSI})_2$ dissolved in acetonitrile, seems not be a critical concern.^[79] The scientific community tends to develop electrolytes that enable the electrochemistry of Mg

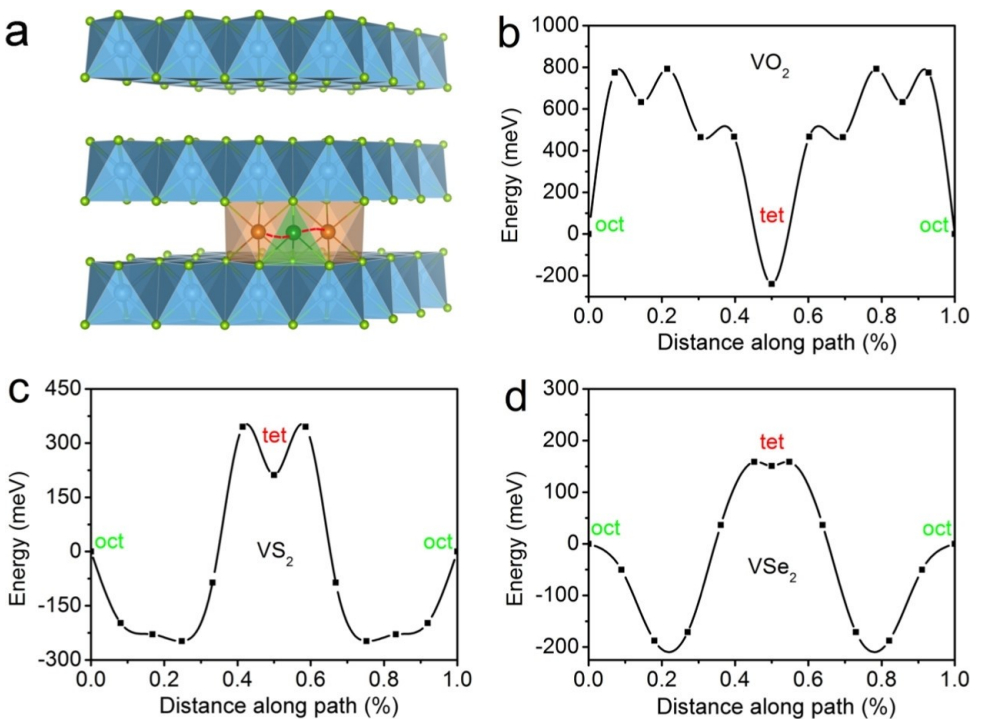


Figure 3. a) Crystal structure of layered MX₂ (M=Ti, V; X=O, S, Se). Ti or V atoms (blue) are at the center of octahedra constructed of X atoms (green). Mg²⁺ migrates between the empty interlayer octahedral sites (orange) through the intermediate tetrahedral sites (olivine), which is marked in red dashed line. Calculated energy barrier for the migration of Mg²⁺ in layered structure along the minimum energy path as obtained by first-principles nudged elastic band (NEB) in calculations. b) VO₂, c) VS₂, and d) VSe₂ within the dilute limit of cation insertion. Reprinted from Ref. [78] with permission. Copyright (2019) American Chemical Society.

anode but, in most cases, without fulfilling the requirements for a good performance of the cathode material.^[80] This approach is fully justified when taking into consideration the high specific capacity that the alkali earth metal possess, but falls short in pursuing the “whole picture” of an alkali-earth metal full battery.

The development of high-energy and high-voltage LIBs has been possible thank to the development of *proper* anode and cathode materials. It is clear that to improve the cell energy, two combined approaches can be followed. In fact, the energy of a cell is proportional to the amount of stored charge Q (Ah) and to the cell voltage (V), which, in turn, is given by the difference in potential of the cathode and that of the anode. Therefore, positive and negative electrode materials with high capacities will increase the overall stored charge Q. On the other hand, cell voltage can be increased by designing high-potential cathodes and low potential anodes.

In Figure 4, a summary of specific capacity vs voltage for a series of materials in RMBs, is reported. The first cathode material used in combination with Li metal was TiS₂, giving a cell voltage of 2.20 V.^[81] TiS₂ was also investigated for Mg²⁺ intercalation, showing a modest specific capacity of 120 mAh g⁻¹ and a low cell voltage of 1.25 V.^[81,82] However, the discharge voltage is not only governed by the cathode material but also by the anode material, the electrolyte, interfacial processes, and the diffusion or migration barriers experienced by divalent cations into the cathode crystal lattice. Cathode materials need to be designed in order to provide the best

parameters for high performance, such as: i) high operating potential and specific capacity, ii) fast and reversible kinetics of Mg²⁺ ions diffusion, iii) good cycling stability. In terms of their storage mechanism, cathode materials are mainly divided into insertion-type and conversion-type cathodes. In this section, a brief overview of the recent progress on cathode host material for Mg²⁺ insertion will be presented, as well as selected cathode materials for practical applications.

4.1. Layered Materials

The structural flexibility of layered materials to accommodate structural deformations due to the insertion of multivalent cations, gives them an advantage as materials of choice for high charge density cations such Mg²⁺ or Ca²⁺. Moreover, layered materials show 2D diffusion channels and high electronic conductivity, providing a favorable framework for Mg²⁺ diffusion and kinetics. There are several types of layered structures potentially able to intercalate Mg²⁺ (See Figure 5), which include layered transition metal oxides, transition metal sulfides, carbides, selenides, molybdenum oxides, manganese oxides, T-based sulfide, layered VOPO₄ species and layered ammonium bronzes.

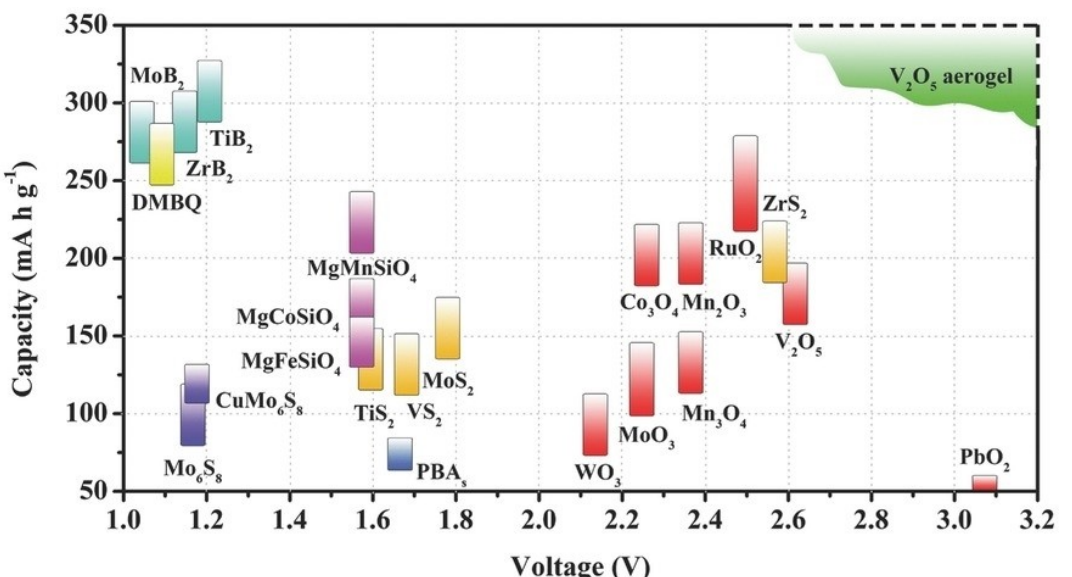


Figure 4. Capacity versus voltage for the reported electrode materials for secondary Magnesium batteries. Reprinted from Ref. [83] under the terms of the Creative Commons CC BY license. Copyright (2016) The Authors.

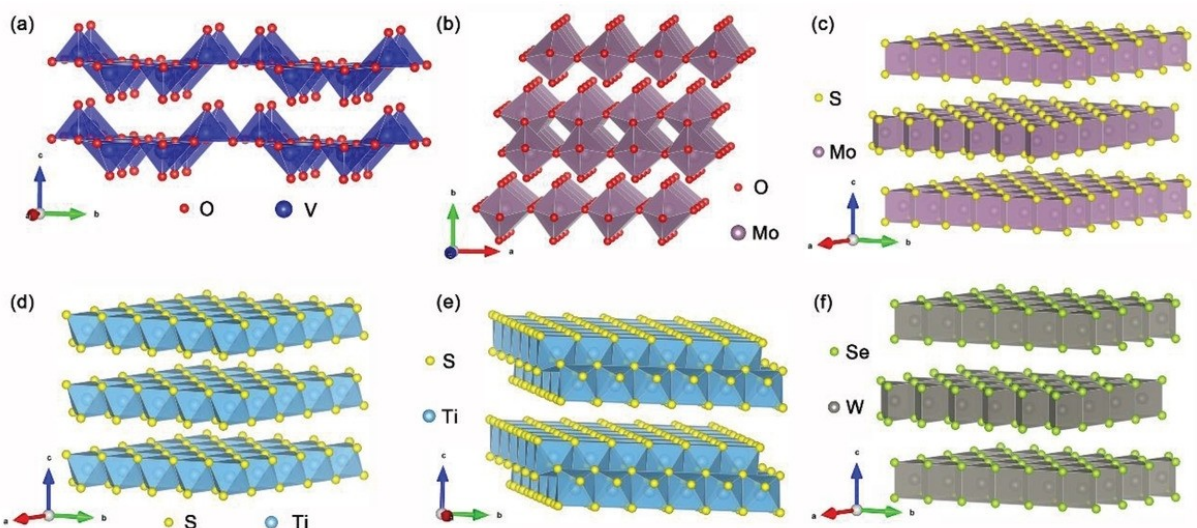


Figure 5. Crystal structures of some layered cathode materials of multivalent rechargeable batteries. Reprinted from Ref. [44] with permission. Copyright (2019) Wiley-VCH.

4.1.1. Layered Transition Metal Oxides

Cathodes based on layered metal oxides show high theoretical insertion potentials and capacities, and a high ratio of intercalant.^[77,84] Among layered transition metal oxides, V₂O₅ has been historically one of the most representative materials. Layered Molybdenum oxides (MoO₃) offer the highest theoretical capacity with ~372.3 mAh g⁻¹ by inserting the Mg²⁺ cation.^[42]

As mentioned above, layered V₂O₅ is one of the most investigated materials, albeit it possesses poor Mg²⁺ intercalation kinetics into orthorhombic 2D diffusion channels.^[85,86] To tackle this issue, different approaches have been used to

improve Mg²⁺ diffusion, such as nanosizing, solvent (H₂O) co-intercalation or high temperatures.^[56,85,87,88] In fact, high capacity of more than 170 mAh g⁻¹ was obtained at room temperature using H₂O co-insertion as charge-shielding approach.^[88] It is worth noting that V₂O₅ with an interlayer space of ~4.37 Å^[89] can also intercalate several other cations (monovalent or multivalent) such as Li⁺, Ca²⁺, Na⁺, K⁺, Ba²⁺, Zn²⁺, Ni²⁺ and it has often been used as test cathode material for metal-ion battery concepts. V₂O₅ has been subject of many theoretical investigations in terms of calculations and modelling, with a benchmarking^[90] perspective. Orthorhombic V₂O₅ undergoes a phase transition during Mg²⁺ insertion, from α - to δ -phase, defined by the stoichiometry of Mg (x_{Mg}) in the cathode

structure.^[90] Calculations suggested that, considering theoretical insertion potentials and phase stabilities, V_2O_5 should remain in the α polymorph during Mg^{2+} insertion.^[90] However, at $x_{Mg}=1.0$ the δ -phase is thermodynamically stable and chemically synthesizable.^[91] This suggests a synthesis preparation of Mg - V_2O_5 cathode in a discharged form as observed for LIBs.^[42] V_2O_5 has a calculated open circuit potential of 3.06 V vs. Mg/Mg^{2+} .^[92] As mentioned above, it undergoes phase transitions during the Mg^{2+} intercalation/extraction (Figure 6a) depending on the stoichiometric ratio of intercalated Mg^{2+} ions (marked as x_{Mg}): starting from α - V_2O_5 to ϵ - V_2O_5 at $x=0.5$ (partially discharged state) and then to δ - V_2O_5 (fully discharged state). These phase transitions are supposed to be reversible.^[92,93] Various experiments with V_2O_5 -based cathodes shown high discharge capacity, at almost ~ 540 mAh g⁻¹, which is one of the highest values of Mg-intercalation ever claimed. This performance was obtained with $Mg(ClO_4)_2$ in ACN.^[94,95] However, this claimed discharge performance was obtained by means of Mg - H_2O co-intercalation, where either wet aprotic electrolytes or hydrated V_2O_5 phases (Xerogel- V_2O_5 , see Figure 7) are incompatible with a Mg metal anode. On other hand, this electrochemical performance of reversible Mg^{2+} insertion, claimed by Lee et al. and Imamura et al., is based on an electrochemical investigation which needs a complementary systematic material characterization.^[95,96] So far, investigations of Mg^{2+} insertion into V_2O_5 and the rest of the scientific

literature, cannot still clearly describe whether Mg^{2+} can be reversibly intercalated for a prolonged number of cycles. Multiple reports tried to address this issue, highlighting the need to decouple side processes such as, proton intercalation, electrolyte decomposition and pseudo-Faradaic reactions that could significantly affect the interpretation of the observed electrochemical processes.^[42]

Recently, a V_2O_5 -PEO nanocomposite was firstly prepared using an in-situ sol-gel method, which showed five-fold capacity enhancement towards Mg^{2+} insertion.^[98] In the nanocomposite structure, the Mg^{2+} diffusion coefficient resulted to be enhanced due to the shielding effect of PEO. V_2O_5/C composites were also used to reversibly insert/extract Mg ions, and they were characterized by a larger interlayer spacing compared with carbon-free V_2O_5 xerogels. This shortens the diffusion path of Mg^{2+} ions, thereby improving electrochemical performance.^[94] A solvothermal method was used to synthesize a graphene oxide (GO)/ V_2O_5 composite as cathode material, with a high discharge capacity up to 178 mAh g⁻¹.^[99]

Another promising cathode material for multivalent-ion insertion, is a MnO_2 polymorph which shows high operating voltage ~ 2.80 V vs Mg/Mg^{2+} (Ag/AgCl reference electrode and calibrated vs. Mg/Mg^{2+} , Mg counter electrode).^[100] MnO_2 can exist in Hollandite (α - MnO_2), water containing- MnO_2 layered- δ and the λ - spinel phases (see Figure 8).^[100-103] As reported, δ - MnO_2 layered oxide, or Birnessite, is a hydrated layered

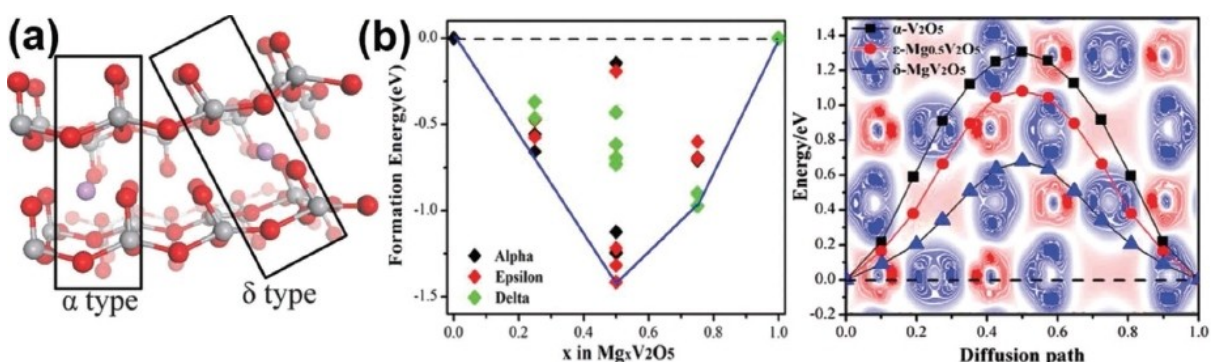


Figure 6. a) Schematic diagram of the α - V_2O_5 to δ - V_2O_5 transformation. Reprinted from Ref. [92] with permission. Copyright (2014) Royal Society of Chemistry. b) Formation energy at different concentrations and migration energy of Mg atoms in different V_2O_5 polymorphs. Reprinted from Ref. [93] with permission. Copyright (2018) American Chemical Society.

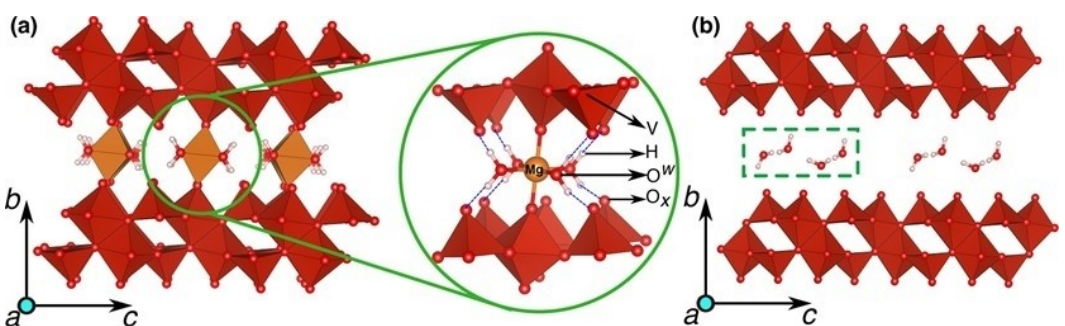


Figure 7. The structures of the fully magnesiated ($x_{Mg}=0.5$) and the fully demagnesiated xerogel structures, with $1H_2O$ per formula unit of V_2O_5 are displayed in (a and b), respectively. A closer view of the Mg coordination environment in the xerogel is displayed within the green circles of (a, b) Reprinted from Ref. [97] with permission. Copyright (2016) American Chemical Society.

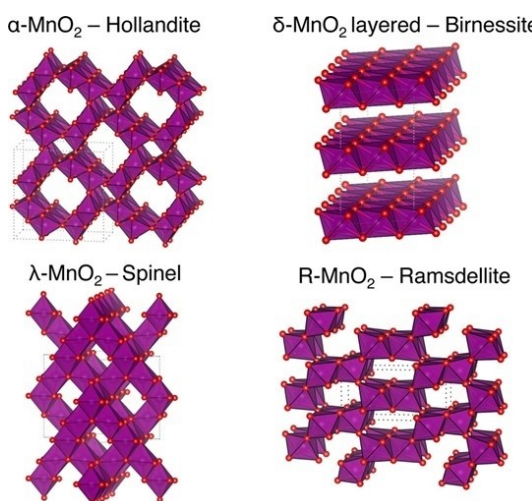


Figure 8. MnO_2 polymorphs investigated as intercalation cathode materials for Mg-ion batteries. MnO_6 octahedra in violet share oxygen (in red) corners and edges in Hollandite $\alpha\text{-MnO}_2$ and Ramsdellite R-MnO_2 and only edges in Spinel $\lambda\text{-MnO}_2$ and Birnessite $\delta\text{-MnO}_2$. Reprinted from Ref. [42] with permission. Copyright (2017) American Chemical Society.

polymorph used to intercalate multivalent cations.^[42] This species was early investigated by different research groups, mostly operating in a water containing electrolyte like $\text{Mg}(\text{ClO}_4)_2/\text{CAN:H}_2\text{O}$ or in aqueous electrolyte.^[100,102] Water molecules improve the migration of Mg^{2+} by shielding the divalent charge. With high reversibility (over 5000 cycles) of Mg intercalation and high capacity ($\sim 231 \text{ mAh g}^{-1}$) it was not clearly elucidated whether or not this good performance could be due to proton co-intercalation.^[100] Clearly, it comes from experimental evidence that this cathode is much more compatible with water containing or aqueous electrolytes. In non-aqueous electrolytes, Mg^{2+} intercalation or migration can be possible, but with slow kinetics compared to the water-containing electrolyte and after a so-called conditioning step in 0.25 M $\text{Mg}(\text{TFSI})_2$ in diglyme.^[100,102] In addition, using this Birnessite cathode and water-containing electrolytes mostly leads to the passivation of Mg metal, if used as reference electrode since the release of the water diffuse could not be excluded, thus creating a passivation film.^[102] As mentioned,

this cathode is a polymorph cathode material, which undergoes reversible transformations from layered to spinel structures.^[100,102] Analogous phase transformation have been observed in LiMnO_2 .^[104] Layered MnO_2 materials have low cost and are environmentally friendly. However, the superior electrochemical performance of layered manganese oxides was achieved by introducing water in RMB systems. Unfortunately, both water in the electrolyte and structural water are incompatible with Mg metal anode.

Orthorhombic $\alpha\text{-MoO}_3$ with layered crystal structure has also been considered as a potential cathode material for RMBs, and was firstly investigated in 1995.^[105] The inserted Mg^{2+} occupied the sites within and between $\alpha\text{-MoO}_3$ layers running along the c-axis. Concerning V_2O_5 , the predicted migration barrier of $\sim 880 \text{ meV}$, is much higher than the Lithium calculated threshold ($\sim 525 \text{ meV}$) indicating a possibly sluggish kinetic behavior.^[56,106,107] Compared to V_2O_5 , the potential difference between the magnesiation and de-magnesiation processes of $\alpha\text{-MoO}_3$ indicates a greater kinetic limitation, which is illustrated by the large overpotential and some degree of irreversibility. This can be due to the potential-induced structural damage, lower electronic conductivity of demagnesiated MoO_3 and some possible conversion reactions at the surface.^[51,56,105] However, $\alpha\text{-MoO}_3$ showed poor electrochemical performance, mainly due to the slow diffusion of Mg^{2+} which can be improved by reducing the particle size of cathode material.^[56] Therefore, a thin film $\alpha\text{-MoO}_3$ electrode (nanoscale thickness and particle size) was synthesized via electrodeposition technique and showed a high reversible discharge capacity of 220 mAh g^{-1} and a discharge potential of about 1.7 V vs Mg/ Mg^{2+} . AC cloth as counter and pseudoreference electrode were used and the potential of the AC pseudoreference calculated as 2.38 V vs Mg/ Mg^{2+} after calibration.^[56]

Fluorinated MoO_3 , e.g. $\text{MoO}_{2.8}\text{F}_{0.2}$, was used to enhance the kinetics of Mg insertion. Fluorine increases the electronic conductivity by liberating an electron, which is delocalized over the entire Mo–O layer, and this contributes to the accommodation of the charge introduced by Mg^{2+} . Therefore, the migration barrier reduces to $\sim 490 \text{ meV}$, and higher discharge capacity and better cycling stability than the MoO_3 are obtained (see Figure 9).^[51] Similar to $\alpha\text{-MoO}_3$, when embedded

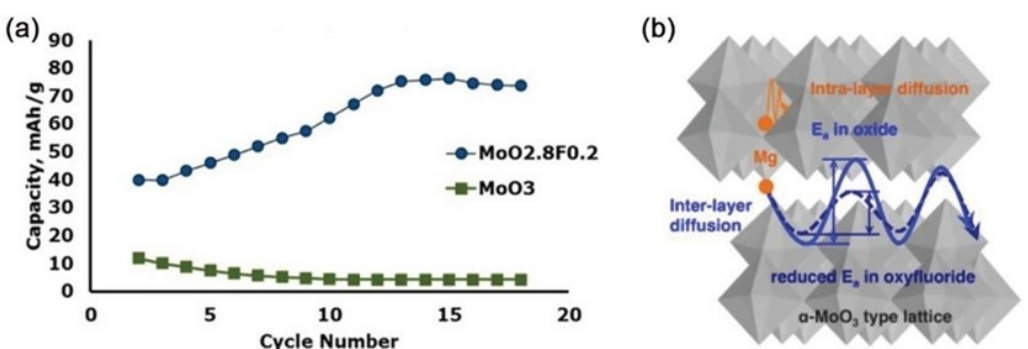


Figure 9. a) Cycling performances of MoO_3 and $\text{MoO}_{2.8}\text{F}_{0.2}$. Reprinted from Ref. [51] with permission. Copyright (2015) American Chemical Society. b) The activation energy of Mg^{2+} diffusion. Reprinted from Ref. [106] with permission. Copyright (2016) American Chemical Society.

into $\text{MoO}_{2.8}\text{F}_{0.2}$ material, Mg^{2+} ions will occupy the space within the $\text{MoO}_{2.8}\text{F}_{0.2}$ layers and move along the axial direction, which is beneficial in reducing the migration barrier.^[106] Kaveevivitchai and Jacobson presented an orthorhombic molybdenum-vanadium oxide ($\text{Mo}_{2.5+y}\text{VO}_{9+\delta}$) as Mg-storage material. $\text{Mo}_{2.5+y}\text{VO}_{9+\delta}$ with an open tunnel structure can improve the diffusion kinetics of Mg^{2+} ions in the layered oxide.^[108] The $\text{Mo}_{2.5+y}\text{VO}_{9+\delta}$ possesses a complex layered structure by sharing corners, to obtain a framework with different membered (three, six, and seven) ring tunnels. These ring tunnels can promote the migration of Mg^{2+} and avoid volume expansion.^[109] Besides, in $\text{Mo}_{2.5+y}\text{VO}_{9+\delta}$, Mo and V ions can exist in several different oxidation states, but always keeping the electroneutrality of electrode material during intercalation of Mg^{2+} ions.^[108] An initial discharge capacity of 397 mAh g^{-1} can be achieved at a low C-rate of C/70.^[108]

4.1.2. Layered Transition Metal Sulfides

The first insertion sulfide cathode material investigated to intercalate Mg^{2+} was a layered structure cathode, TiS_2 .^[42] The substitution of O by S (from anatase TiO_2 to TiS_2 for example) in layer structured materials makes longer Mg–S chemical bonds, weakens the interaction strength between Mg^{2+} ions and host lattice, and therefore, enlarges the channel for Mg^{2+} ions diffusion and increases the mobility of Mg^{2+} . This causes a decrease of the migration barriers, as well as a decrease in the operating voltage, when compared to layered transition oxides.^[110] TiS_2 is a typical example of cathode material, which can exist in a dual stable phase, and undergoes reversible phase transformation, from layered to spinel phase. Other viable sulfide-based cathode layered materials are NiS , Cu_2S .

The early study of reversible magnesiation of TiS_2 showed low discharge capacity even at 60°C (20 mAh g^{-1}) with no structural evidence for the intercalation of Mg^{2+} .^[75,111] Later, an initial capacity of $\sim 270 \text{ mAh g}^{-1}$ from a micrometer-sized material was obtained, even with a high Mg migration barrier

of 1200 meV, which defines, at 60°C , very sluggish kinetics of Mg diffusion.^[82,112] To tackle this issue, shielding agents like chloride ions were used to reduce the charge density of the Mg cations (See Figure 10). Room temperature experiments showed an initial discharge capacity of 239 mAh g^{-1} , whereas higher capacity of 450 mAh g^{-1} was achieved at 60°C .^[113] Similar issues were described for MoS_2 , another widely studied candidate cathode material, showing a high theoretical migration barrier (2.61 eV).^[114] Organic molecules were also used to increase the interlayer space, as demonstrated by Liang et al.^[20] and therefore to alleviate the diffusion barrier ($\sim 0.97 \text{ eV}$), improving the capacity in MoS_2 (from $\sim 20 \text{ mAh g}^{-1}$ for pristine- MoS_2 to $\sim 80 \text{ mAh g}^{-1}$ with polymer intercalated MoS_2).^[20] The polymer molecules (e.g., polyethylene oxide, PEO) were inserted to push apart the MoS_2 layers.

As many other Mg^{2+} insertion investigations, the actual insertion of Mg^{2+} has not clearly been demonstrated with appropriate structural characterization tools (e.g., XRD), and a degree of uncertainty whether they can be appropriate cathode material for Mg intercalation^[20,115,116] still clouds further research. An average specific capacity of 170 mAh g^{-1} with an operating voltage of 1.80 V vs. Mg/Mg^{2+} (ultrasmall Mg particles as anode) was obtained using graphene-like MoS_2 (G- MoS_2) as cathode material synthesized by a solvothermal method.^[116] MoS_2 nanoribbons were also considered with some reserve as a good potential cathode material for Mg insertion thanks to its multilayer structure, which can increase the active area, hence a considerable theoretical capacity of 223.2 mAh g^{-1} can be obtained.^[114] Recently, a vanadium sulfide-based material, VS_4 ^[117] with special 1D atomic-chain structure showed promising performance as intercalation cathode for Mg-ion batteries. An excellent initial discharge capacity of 251 mAh g^{-1} at 100 mA g^{-1} specific current was demonstrated. A remarkable long-term cycling with high capacity retention (74 mAh g^{-1} after 800 cycles) at 500 mA g^{-1} , was also reported.^[118]

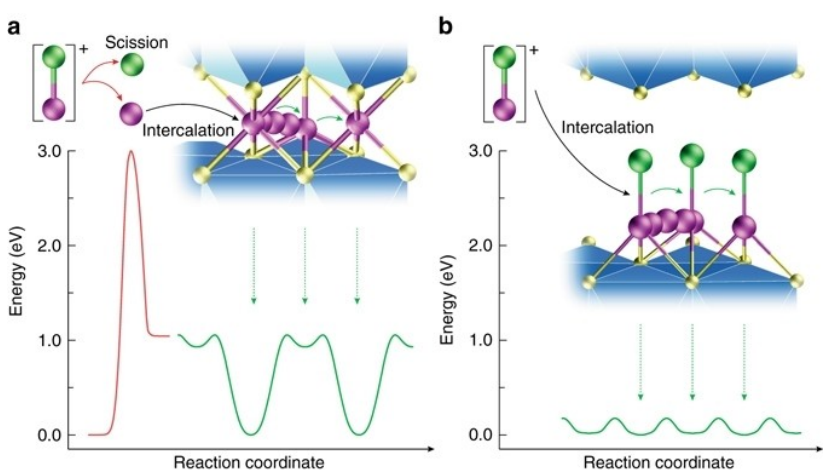


Figure 10. The activation energy for intercalation and the migration energy barrier for diffusion of Mg^{2+} (a) and MgCl^+ (b), with schematic illustrations of intercalation in the insets. Reprinted from Ref. [113] under the terms of the Creative Commons CC BY License. Copyright (2017) The Authors.

4.1.3. Layered Transition Metal Carbides or MXenes

MXene materials have a similar structure to V_2O_5 and MoS_2 , with the chemical formula $M_{n+1}X_nT_x$ (M =an early transition metal element, X is C or N, T_x represents OH^- , O^{2-} , F^- and other surface functional groups, $n=1-3$). MXene materials were predicted firstly to reversibly intercalate Mg^{2+} by Islam and Eames.^[119] MXene materials showed negligible Mg storage capacity, therefore a MXene cathode material was developed by pre-intercalation of a cationic surfactant (cetyltrimethylammonium bromide, CTAB).^[120,121] Compared with the pure $Ti_3C_2T_x$, the $Ti_3C_2T_x/CTAB$ showed a high volumetric specific capacity of 300 mAh cm^{-3} .^[121] Electrostatic self-assembly technique was used to prepare a sandwich-structured MXenes@C nanosphere composite cathode material with increased layer spacing and specific area, providing a channel for reversible intercalation/extraction of Mg^{2+} and improved performance.^[122] Recently, the flexible and conductive 3D macroporous $Ti_3C_2T_x$ MXene films as a cathode for Mg exhibited desirable cycling stability and excellent rate performance.^[123] It is worth noting that MXenes are used to design hybrid magnesium/lithium-ion batteries with excellent performance.^[124]

4.1.4. Layered Transition Metal Selenides

Layered selenide oxides allow fast Mg^{2+} diffusion with low migration barriers, higher electronic conductivity and weaker electronic interaction between intercalant and layered anion compared to the layered sulfide and oxide. However, layered selenides hold a low operation potential like Chevrel Phase cathodes compared to layered oxides.^[45,125,126] It was reported that Mg^{2+} can reversibly intercalate/deintercalate into/from WSe_2 nanowires (7–100 nm) which promote Mg^{2+} diffusion and enhance interface contacts between the electrode and the electrolyte.^[127] With a WSe_2 nanowire-based electrode, a high initial discharge capacity of about 220 mAh g^{-1} at 50 mA g^{-1} , superior cycling stability (203 mAh g^{-1} after 160 cycles), and good rate performance (142 mAh g^{-1} at 800 mA g^{-1}) were reported.^[127] However, the synthesis of WSe_2 nanowires is complicated. Thus, finding a facile way to prepare WSe_2 is necessary. To date, only few-layered selenides were applied to RMBs. Layered $TiSe_2$ used as a cathode material in SIBs was identified as potential candidate to intercalate Mg^{2+} ions. The Mg-battery with layered $TiSe_2$ as cathode and Mg metal exhibited a discharge specific capacity of 108 mAh g^{-1} with a potential plateau at about 1.0 V vs. Mg/Mg^{2+} (Mg metal as anode-3 electrode setup) with $Mg(AlCl_2EtBu)_2/THF$ as electrolyte. Theoretically, 0.83 moles of Mg can be embedded in each $TiSe_2$ lattice. However, only 0.41 moles in practical test^[126] were reported.

4.1.5. Layered VOPO₄ and Layered Ammonium Bronze

Mg^{2+} cation can be also intercalated into layered VOPO₄. Showing a structure characterized by corner-sharing VO₆

octahedra and PO₄ tetrahedra, VOPO₄ is seen as a promising candidate.^[59,128] VOPO₄ nanosheets with expanded interlayer spacing (from 0.74 to 1.42 nm) obtained by displacement reaction with phenylamine (PA) molecules showed superior rate capability (109 mAh g^{-1} at 2000 mA g^{-1}) and good cycling stability (192 mAh g^{-1} after 500 cycles at 100 mA g^{-1}) when MgCl⁺ was intercalated.^[128] Benefiting from the increased layer distance, fast ion diffusion kinetics and the MgCl⁺ intercalation with low polarization, allowed to achieve an outstanding electrochemical performance.^[128] Unfortunately, using a water-activated layered-structure VOPO₄, where H₂O molecules are used to smoothen the solid-state diffusion of Mg²⁺ cations, does not show encouraging results.^[59] Using a hydrothermal reaction, ammonium ions can be used to increase the interlayer space, and the NH₄V₄O₁₀ cathode showed an initial discharge capacity of 174.8 mAh g^{-1} with an average discharge potential of ~2.31 V vs. Mg/Mg²⁺ in 0.5 M Mg(ClO₄)₂/ACN electrolyte.^[55] The measurements were conducted in a 3-electrode cell setup using AC counter and quasi-reference electrodes, the latter calibrated vs. Mg/Mg²⁺. The reversible Mg storage mechanism of the layered NH₄V₄O₁₀ was demonstrated by XRD, Fourier Transform Infrared (FTIR) spectroscopy, X-ray Photoelectron Spectroscopy (XPS), and Inductively Coupled Plasma-Optical Emission Spectroscopy (ICP-OES). Literature data shows that the NH⁴⁺ cation in the interlayer space of NH₄V₄O₁₀ is important for stabilizing the crystal structure.^[44]

4.2. Polyanionic Structures

Polyanionic structures represent a wide class of cathode materials, which have been explored, in the beginning, as cathodes for LIBs.^[129] Due to the extensive research efforts, polyanionic frameworks are nowadays one of the three fundamental and most studied material class.^[130] The development of alternative monovalent ion-based battery chemistries, such as SIBs, further stimulated the interest in these structures.^[131] More recently, the effort to push the advent of multivalent battery chemistries induced researchers to explore the possibility to reversibly intercalate-deintercalate divalent ions into these materials.^[110]

Inside this class of materials different structural types can be found, like olivines, NASICON-type and fluorophosphates. Among them, one of the most widely explored category as candidate cathode material, historically, is represented by olivines, in which are present non-toxic, cheap and abundant materials like transition metal MPO₄ phosphates and MSiO₄ silicates (M =transition metal). In particular, one of the most attracting features of transition metal silicates for battery scientists is the possibility to (theoretically) undergo a two electrons redox reaction thus providing large specific capacities (See Figure 11).

Olivines crystallize in the orthorhombic system (Space groups $Pnma$ and $Pnmb$) and are generally addressed as MXO₄ (M =Fe, Mn, Co -X=P, Si). These structures are characterized by an array of MO₆ corner sharing transition metal octahedra, which, in turn, share corners and edges with XO₄ tetrahedra.

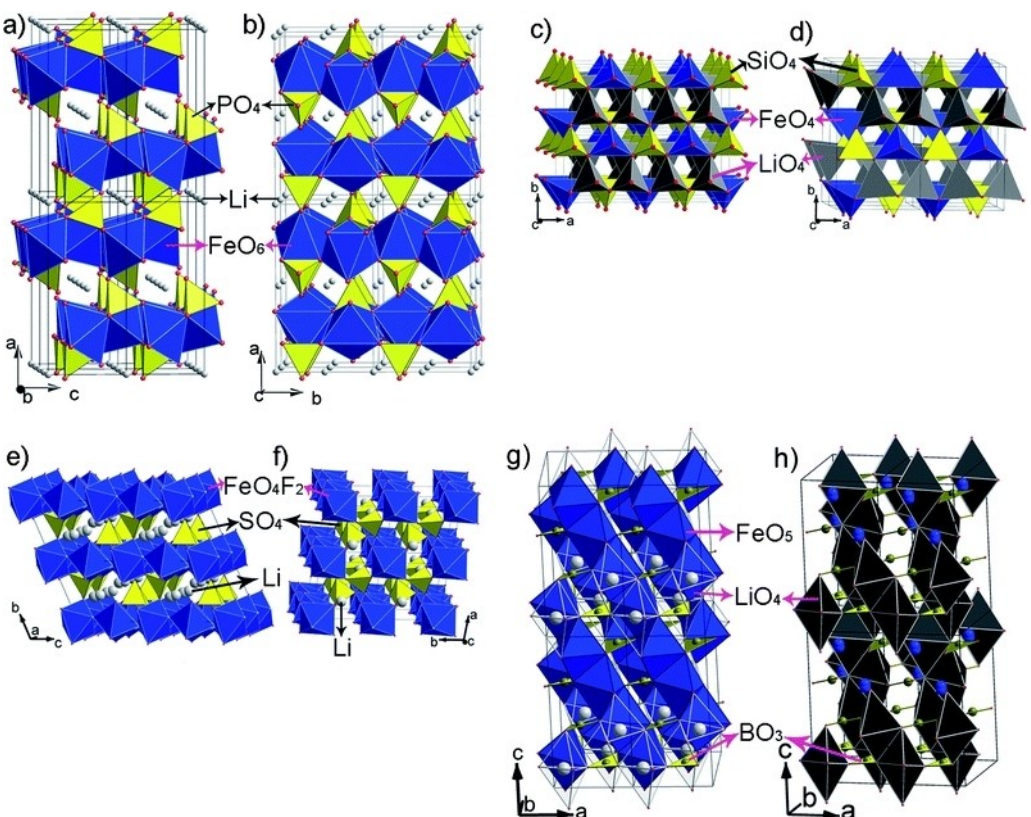


Figure 11. Polyhedral representation of the crystal structure of some typical polyanion-type cathode materials. a) and b) Olivine LiFePO_4 viewed along the b - and c -axis, respectively. Yellow tetrahedral, PO_4 ; blue octahedral, FeO_6 . c) $\text{Li}_2\text{FeSiO}_4$ (space group $Pmn2_1$) viewed along the c -axis; d) $\text{Li}_2\text{FeSiO}_4$ (space group Pmn) viewed along the a - and b -axis. Grey tetrahedral, LiO_4 ; blue tetrahedra, FeO_4 ; yellow tetrahedra, SiO_4 . e) and f) LiFeSO_4F viewed along the a - and c -axis, respectively. Yellow tetrahedral, SO_4 ; blue octahedral, FeO_4F_2 ; Li distribution between two half-occupied positions is disordered. g) LiFeBO_3 viewed along the b -axis; h) LiFeBO_3 viewed along the b -axis with FeO_5 bipyramidal not indicated, possible Li diffusion pathways parallel to the c -axis are showed. The paired face-sharing LiO_4 tetrahedra are shown in grey (lithium statistically occupies two tetrahedral sites, statistically alternate positions of Li are not indicated for simplicity), trigonal FeO_5 bipyramids are shown in blue (iron statistically occupies two trigonal sites), BO_3 triangles are shown in yellow. Reprinted from Ref. [132] with permission. Copyright (2011) Royal Society of Chemistry.

The result is the presence of two non-equivalent sites (M1 and M2) available for metal cations.^[133] Due to the nature of their structure, electron delocalization in olivine-type materials is difficult and olivines often suffer of poor electronic conductivity.^[129] Moreover, the slow Mg^{2+} diffusion originating from its high charge density poses a non-trivial scientific challenge, in order to enable fast and reversible insertion during electrochemical cycling.

In the first place, since theoretical studies are becoming more widespread and reliable, they represent a powerful and fast screening tool to probe already known and new materials for Mg-intercalation. In this regard, theoretical studies, which are becoming more and more popular, based on first-principle calculations of thermodynamic properties of selected materials, can help to speed up the screening process, and to evidence discrepancies with the reported experimental data. Ling et al.^[134] reported a DFT study on the thermodynamics of the magnesiation process of manganese-based olivine materials, predicting similarities with Li-ions insertion. Using MgMnSiO_4 as model compound, the authors predicted a two-step reduction of the transition metal upon Mg insertion, with the electron transfer occurring between Mg and Mn/O ions of the $\text{Mn}_4\text{Si}_4\text{O}_{16}$

unit. The two-step approach was extended to other silicates and phosphates (Co, Ni, Fe) with consistent results. This two-step mechanism translated in the prediction of two plateaus for electrochemical Mg insertion at different potentials, in the range of 3.00 V–4.00 V vs Mg/Mg^{2+} , though severely limiting the choice of a viable electrolyte for electrochemical testing.

Among magnesium silicate materials MgMSiO_4 , those based on M=Fe, Co, Mn have received the most attention from the scientific community and their exploration is now undergoing. One of the potential disadvantages of silicate-based materials, other than sluggish kinetics of Mg^{2+} insertion extraction, is represented by a certain degree of anti-site mixing between M1 and M2 sites, which leads to increased disorder and thus possible hampering of electrochemical activity.^[135] In this regard, several years ago, Redfern et al.^[136] proposed a model that correlates cation ordering and natural occurring olivine cooling rates as a means to date the earth mantle composition, from which interesting cues could be obtained to limit the anti-site effect that could hamper Mg^{2+} insertion in olivines.

Investigations of iron silicates for multivalent cation insertion have been conducted starting from the available data on LIB research. A favorable electrochemical delithiation

strategy has been reported by Orikasa et al.^[60] (Figure 12), from which the obtained metastable FeSiO_4 phase was explored for Mg^{2+} insertion, showing high specific capacity values, supporting their findings with XRD and XANES data. The authors assigned this high degree of magnesiation to the intrinsic properties of the 3-D conduction framework of the delithiated FeSiO_4 phase, characterized by a slightly distorted SiO_4 tetrahedra arrangement and Fe atoms being in a tetrahedral coordination environment, rather than octahedral.

Reports of theoretical investigations,^[137] combining several modeling techniques showed a preferred diffusion path for Mg^{2+} along 1-D tunnels along the c-axis of the MgFeSiO_4 unit cell, which show the lowest activation energies. Predicted diffusion coefficients were in the range of 10^{-9} , but an experimental confirmation is still missing at the time of writing. The reported theoretical potential trends,^[137] are in accordance with literature data.^[60,134]

Mn-based silicate MgMnSiO_4 also attracted attention as candidate cathode material. Several synthesis procedures have been employed to prepare the $\text{Mg}_{1.03}\text{Mn}_{0.97}\text{SiO}_4$ silicate, from solid state reaction to hydrothermal,^[138–141] and from the resulting variety of morphologies and particles sizes, a lower annealing temperature and mesoporous morphology were found to be the best combination to improve Mg^{2+} insertion kinetics. Insertion voltages were found to be located at 1.60 V and 1.10 V, in contrast to theoretical predictions.^[134]

As already mentioned, antisite mixing has been predicted to have a strong influence on the electrochemical performance of olivine structures. Systematic studies^[135] focused on the

MgMnSiO_4 material, showed a relationship between the annealing temperature and the degree of site mixing inside the crystal structure. By means of XRD, based on the [311]-to-[121] reflection intensity ratio, it was possible to determine the site occupancy of the Mg^{2+} in the M1 olivine site. In addition, sintering temperature can influence the average crystallite size, and samples with a higher degree of cation mixing and bigger crystallite size obtained by sintering at high temperature showed worst performance, while synthesis at 450 °C highlighted a markedly decreased anti-site mixing and improved diffusion by crystallite size in the order of 60 nm–70 nm (See Figure 13).

Magnesium cobalt silicate MgCoSiO_4 has also been investigated in a handful of reports as candidate cathode material for RMBs.^[142,143] As in the case of Mn-based silicate materials, several synthesis methods have been employed to optimize morphology, mostly leading to spherical-shaped particles in the hundreds of nanometers size range.

Further, it is worth noting, that the results of the reported electrochemical investigations, present in some cases remarkable discrepancies in capacity values and voltage/potential profiles, possibly due to different choice of electrolytes and cell setups which are known to be critical in the RMB research field. As an example, Feng et al.^[139] and Truong et al.,^[143] reported remarkable differences in MgMnSiO_4 ($\text{Mg}_{1.03}\text{Mn}_{0.97}\text{SiO}_4$ in the case of Feng) cycling behavior and voltage profiles. The authors used completely different electrolyte systems like 0.25 M $\text{Mg}(\text{AlCl}_2\text{BuEt})_2/\text{THF}$ (Feng) and 0.5 M $\text{MgClO}_4/\text{ACN}$ (Truong), and different counter electrodes, as Mg metal was used by Feng

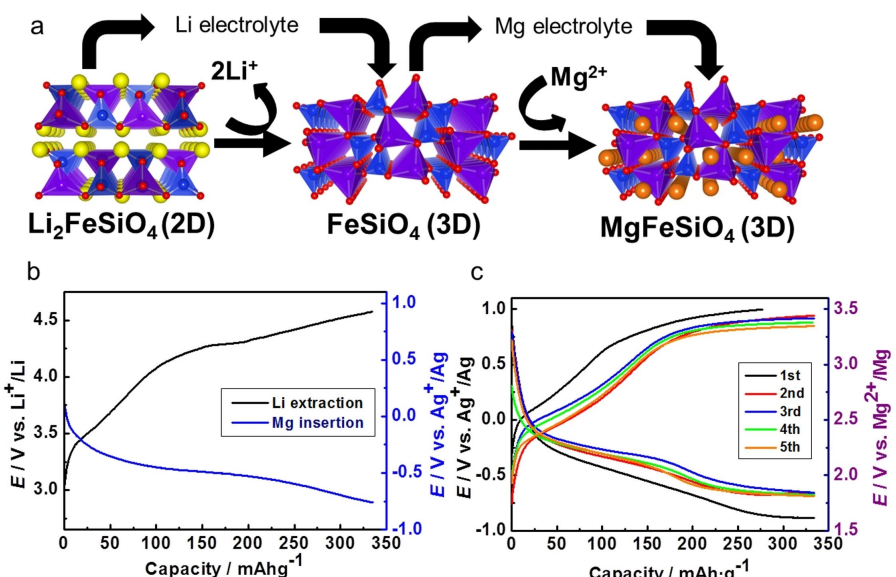


Figure 12. Preparation of ion-exchanged MgFeSiO_4 and charge-discharge profiles. a) Schematic illustration of the ion-exchange methodology for the electrochemical synthesis of MgFeSiO_4 from $\text{Li}_2\text{FeSiO}_4$. Two-dimensional (2D) framework of $\text{Li}_2\text{FeSiO}_4$ and three-dimensional (3D) framework of FeSiO_4 and MgFeSiO_4 . The 3D framework can incorporate Mg ions in the interspace (void). b) Charge-discharge profiles for ion exchange process from $\text{Li}_2\text{FeSiO}_4$ to MgFeSiO_4 . For Li extraction process, two-electrode cells using lithium as counter electrodes were used. Electrolyte was 1 M LiClO_4 in propylene carbonate. For Mg insertion process, three-electrode cells (using Mg metal counter electrode and silver reference electrode) were used. Electrolyte was 0.5 M magnesium (trifluoromethylsulfonyl)imide ($\text{Mg}(\text{TFSI})_2$) in acetonitrile as solvent. Measurement temperature was 55 °C. Current density was 6.62 mA g⁻¹ ($\text{Li}_2\text{FeSiO}_4$). c) Charge-discharge profiles of ion-exchanged MgFeSiO_4 . Three-electrode cells using Mg metal counter electrode and silver reference electrode were used. Electrolyte was 0.5 M magnesium (trifluoromethylsulfonyl)imide ($\text{Mg}(\text{TFSI})_2$) in acetonitrile (solvent). Measurement temperature was 55 °C. Current density was 6.62 mA g⁻¹ (MgFeSiO_4). Reprinted from Ref. [60] under the terms of the Creative Commons CC BY License. Copyright (2014) The Authors.

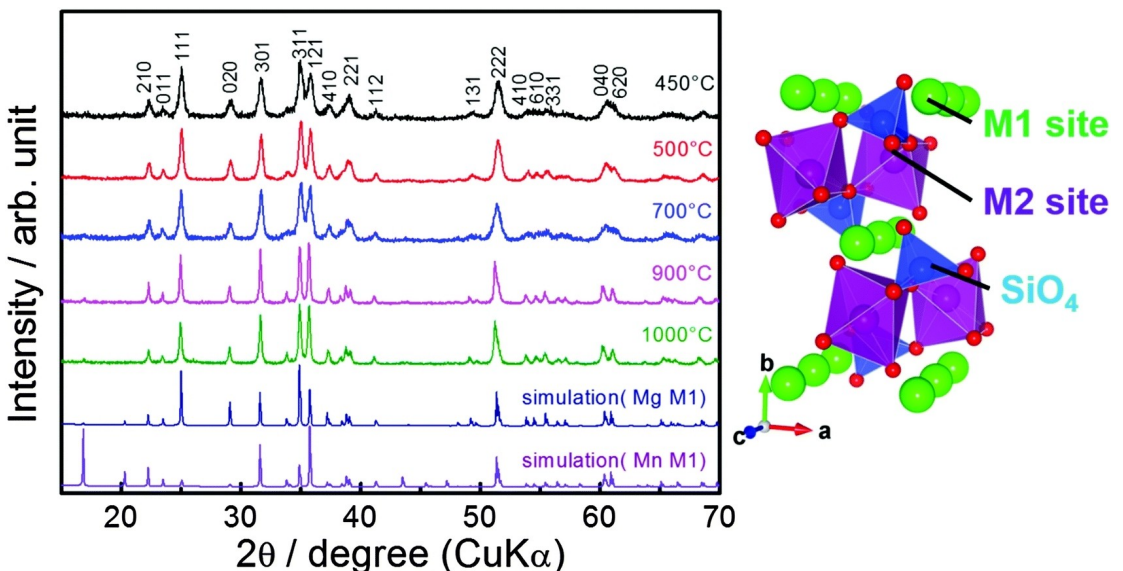


Figure 13. Powder XRD patterns of MgMnSiO_4 synthesized at various temperatures, and schematic projection of olivine-type MgMnSiO_4 visualized using VESTA. Reprinted from Ref. [135]. Copyright (2016) Royal Society of Chemistry.

and activated carbon by Truong in a 2-electrode coin cell setup for cycling tests. These results are also not in agreement with the theoretical investigations from Ling et al.^[134] It is worth underlining again the necessity of consistent electrolyte systems and cell setups in order to be able to compare literature data.

Olivine metal phosphates MPO_4 are a popular sub-class of polyanionic materials, which have been studied quite extensively since the early work of Goodenough et al.^[144] that proposed FePO_4 as a Li intercalation cathode material. In addition, with the work of Armand et al.,^[145] this material was enabled in cycling in an electrochemical Li cell through the implementation of a thin layer of carbon coating to improve, the otherwise low electrical conductivity. The good diffusivity of these materials, in combination with a very low volume variation of the crystal cell during (de)intercalation processes, an inherently high safety and low cost, made them very popular in small scale commercial applications. For these reasons, during the years, research efforts widened their investigations to other metal phosphates as alternative and promising materials with interesting results.^[146] Moreover, with the advent of the Na-ion chemistry, a revamped research interest led to new investigations on these materials.^[147] In view of this, in the quest for new viable candidate materials for RMBs, FePO_4 has been subjected to initial investigations.

Theoretical calculations combined with electrochemical experiments^[148] (See Figure 14) focused on a parallel evaluation between $(\text{Li})\text{FePO}_4$ and $(\text{Mg}_{0.5})\text{FePO}_4$ ion mobility, revealing that for the oxidized state (FePO_4) the migration barrier for Mg is 580 meV, which is a higher value than for Li, but still amenable to let the intercalation process possible. On the other hand, in the magnesiated phase $\text{Mg}_{0.5}\text{FePO}_4$, is predicated to be above the 1 eV threshold, making theoretically impossible the deintercalation of Mg^{2+} . A deviation from the “wave-like” diffusion

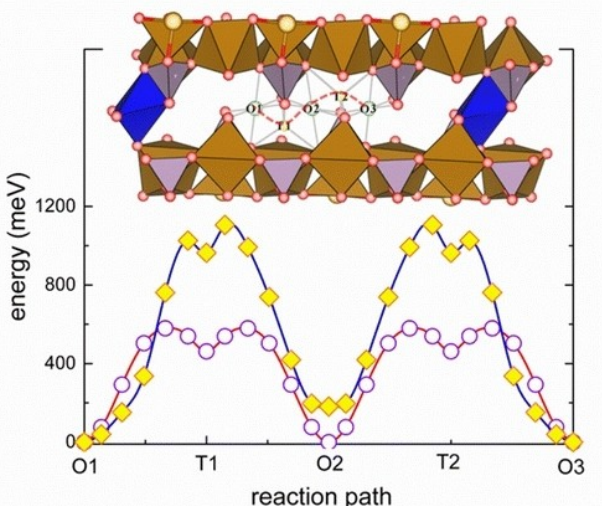


Figure 14. Energy profile for Mg^{2+} to diffuse in olivine FePO_4 (open circle) and $\text{Mg}_{0.5}\text{FePO}_4$ (solid diamond) lattice. (Top insert) Trajectory for a wave-like octahedral–tetrahedral–octahedral path. Red, O; brown, Fe; purple, P; blue, Mg. Reprinted from Ref. [148] with permission. Copyright (2016) American Chemical Society.

path, typical for Li^+ ions, has been indicated as potential factor for this result. The electrochemical insertion reaction of Mg^{2+} , carried out at $20 \mu\text{Acm}^{-2}$ current density showed little to none electrochemical activity.^[148] Investigations by means of TEM, FTIR and XPS analysis, found that a several nanometers thick layer of the surface of FePO_4 particles experienced amorphization, thus impeding any additional electrochemical activity. A successful attempt to synthesize the magnesiated phase $\text{Mg}_{0.5}\text{FePO}_4$, has not been reported in literature yet. This is consistent with calculations^[148] that predicted thermodynamic instability of the magnesium phosphate towards the formation of $\text{Mg}_3(\text{PO}_4)_2$ and $\text{Fe}_3(\text{PO}_4)_2$.

Natrium Super Ionic Conductor, or NASICON, represents a wide category of inorganic solid conductors, with the parent compound being $\text{Na}_{1+x}\text{Zr}_2\text{Si}_x\text{P}_{3-x}\text{O}_{12}$.^[129] The NASICON phase, with the general formula $\text{A}_x\text{MM}'(\text{XO}_4)_3$, generally falls into the space groups R3 (ombohedral) and C2/c (monoclinic), and it is characterized by a 3D framework of MO_6 and $\text{M}'\text{O}_6$ octahedra, which share all their corners with the XO_4 tetrahedra. The repetition of the basic $\text{MM}'(\text{XO}_4)_3$ unit, together with the high degree of covalency, the weaker interactions between the alkali metal ions and the framework, creates the conditions for a fast ion conduction, leading to a versatile class of material, used both as solid state electrolytes and insertion materials.

Reports from the early 2000s^[61,149] explored the possibility of Mg^{2+} ions insertion inside $\text{Mg}_{0.5+y}(\text{M}_y\text{Ti}_{1-y})_2(\text{PO}_4)_3$ NASICON species with $\text{M}=\text{Fe}, \text{Cr}$. Preliminary XRD measurements tried to correlate annealing temperature and variations on the unit cell parameters upon metal substitution. The effects of metal substitution on the discharge plateaus were examined also by electrochemical experiments at low current densities of $j=25 \mu\text{A cm}^{-2}$ hinting at a diffusion-controlled mechanism for the insertion of Mg^{2+} cations.

In more recent reports from Orikasa^[150] and Zeng,^[151] both $\text{Li}_3\text{V}_2(\text{PO}_4)_3$ (LVP) and $\text{Na}_3\text{V}_2(\text{PO}_4)_3$ (NVP) were used as parent compounds to be tested towards the insertion of Mg^{2+} ions, via a previous electrochemical extraction of the alkali metals, as reported in Figure 15. From a structural and morphological point of view, both reports tried to optimize the material by means of a carbon coated composite structure using different synthetic approaches, but showing a similar morphology and particle size distribution. Electrochemical experiments showed slightly different average working potential ranges for the magnesium insertion reaction (2.90 V for LVP and 2.45 V for NVP vs. Mg/Mg^{2+} , respectively). It is worth noting that the deviations in the obtained discharge capacities could be addressed also to remarkably different chosen electrolyte systems. In addition, insertion mechanism was discussed by Zeng^[151] who provided ex-situ XRD and XPS data, together with a preliminary calculation of diffusion coefficients extrapolated

by GITT technique, suggesting a two-phase insertion mechanism.

Recently, transition metal fluorophosphate attracted attention as potential Li^+ and Na^+ cathode insertion materials^[152] due to promising electrochemical properties, a 3D conduction framework and good general stability. It is worth noting that this class of materials do not seem to fall inside a specific structural class, but it is rather showing a quite varied crystallography.

For instance, magnesium iron fluorophosphates (MgFePO_4F) can be synthesized by ball-mill assisted carbothermal route.^[153] Nonetheless, a distorted monoclinic (I2/a) 3D framework, which resulted in the formation of zig-zag chains of distinct sites (M1 and M2), together with anti-site mixing, might determine poor electrochemical performance. These hypotheses were then supported by XRD, theoretical calculations, electrochemical experiments and data elaboration, i.e. differential plots.^[153]

4.3. Spinel-Based Structures

Aurbach et al. investigated the intercalation of Mg^{2+} into the Chevrel phase Mo_6S_8 at a cell voltage of 1.00–1.30 V (Mg CE-2 Electrode Setup) and a theoretical capacity of 128 mAh g^{-1} .^[155] Despite the good cyclability, the low specific capacity and low operating potential of the Chevrel phase Mo_6S_8 hinder its application in RMBs.^[10,156] Oxide spinel structures are well known as suitable host materials for Li-insertion, since they are able to provide fast ion diffusion and are able to operate at high potentials.^[157] However, in terms of specific capacity, LiMn_2O_4 at 143 mAh g^{-1} , is slightly lower than MgMn_2O_4 with $\sim 270 \text{ mAh g}^{-1}$. It has already been shown that the spinel LiMn_2O_4 phase can be electrochemically converted to MgMn_2O_4 by pre-treating it in 0.1 M HCl aqueous solution, in order to remove Li^{+} -ions and afterwards intercalating Mg^{2+} electrochemically, in aqueous electrolyte.^[103]

Zhang et al. were also able to intercalate Mg^{2+} into Mn_2O_4 spinel structure, in an aqueous environment (MgCl_2) with good columbic efficiency and discharge capacity of 546.6 mAh g^{-1} .^[158]

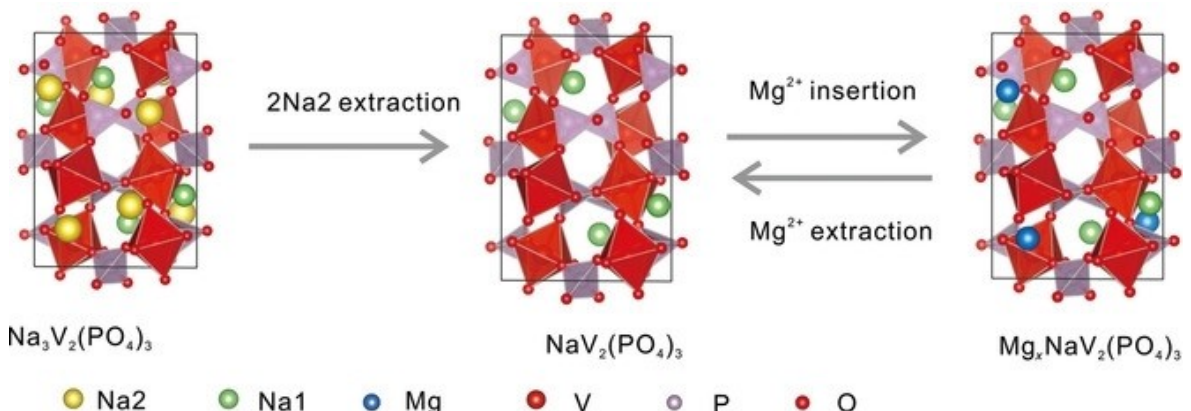


Figure 15. Illustration of the electrochemical desodiation and (de)magnesiation processes. Reprinted from Ref. [151] with permission. Copyright (2017) Wiley-VCH.

Kim et al. also found out that water molecules mostly do not accompany the Mg ions, which means that it should be also possible to intercalate Mg^{2+} in non-aqueous electrolytes, since aqueous electrolytes are not compatible with the Mg metal anode. First attempts in an $Mg(TFSI)_2$ /diglyme or PC electrolytes revealed that a very low degree of Mg^{2+} can be inserted into Mn_2O_4 , compared to aqueous electrolytes. However, a large voltage hysteresis was reported. These issues are mainly addressed to the high kinetic barriers in non-aqueous electrolytes.^[103]

In order to understand the intercalation of multivalent ions into spinel structures, it is important to briefly describe the crystal structure itself. The spinel host material has a general formula of AB_2X_4 and a $Fd\bar{3}m$ space group (Figure 16), in which A is either a monovalent ion or a multivalent ion, and B is a redox active ion like Mn or a mixture of Mn with other cations like Ni or Co.^[154] The anion X can be oxygen to form oxide spinel or divalent S or Se atoms to form thiospinels.^[159] To start with, oxide spinel structures form a cubic-closed-packed (ccp) structure in which the A ions are located at the 8a tetrahedral sites and the B ions are located in alternating octahedral sites along the three crystallographic axes, designated as 16d sites, creating 3D diffusion channels. Additionally, there are empty octahedral sites designated as 16c sites.^[160] In the spinel closed-packed face centered cubic oxygen structures (fcc), Mg^{2+} diffusion follows the lower energy path which crosses through a shared face between tetrahedral sites (tet) and octahedral sites (oct) leading to either tet-oct-tet or oct-tet-oct diffusion topologies, as shown in Figure 2. This finally follows a symmetric path to the next equivalent stable site.^[77] However, it is also known that divalent cations show slower diffusion into the host materials due to stronger cation-anion interaction compared to monovalent ions like Li^+ .

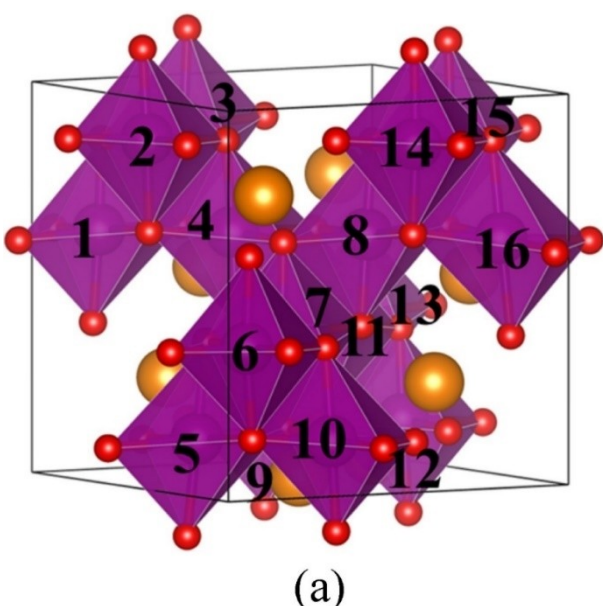


Figure 16. The crystal structures of a) MMO ($Fd\bar{3}m$). The purple octahedrons represent Mn atoms, and the grey octahedrons represent Ni replacement. Reproduced from Ref. [154]. Copyright (2016) Elsevier.

In general, the intercalant mobility is mainly determined by three factors: (1) connectivity between sites; (2) size of the diffusion channel and the intercalant ion; (3) interaction strength between the intercalant and the host structure. Theoretical investigations of Liu et al. of the tetragonal spinel, regarding the migration energy barrier, reveal that Mg^{2+} (600–800 meV) show a higher migration barrier compared to Li^+ (400–600 meV). Usually, as mentioned before, migration barriers of ~525 meV correspond to a typical ionic diffusivity of $10^{-12} \text{ cm}^2 \text{ s}^{-1}$ at RT, which approximately represents the upper limit for reasonable charge/discharge performance. With a smaller particle size, it is able to accept a larger diffusion barrier up to ~645 meV. Since Mg^{2+} insertion barrier value lays above the ideal migration barrier, it does not seem to be a promising insertion type material unless either the particle size is decreased, or the temperature is adjusted. Transition metals like Cr, Ni and Co in the spinel structures allow for slightly lower diffusion barriers. However, Mn-containing spinel structures exhibit higher voltages and higher volumetric capacities, as well as increased stability.^[37]

Improving the crystallite size, which helps to shorten ion transport pathways and improves Mg mobility, is a major aspect. Kim et al. proposed a one-step colloidal synthesis method and observed a nanocrystal $Mg_{0.5}Mn_{2.5}O_4$ spinel structure, showing good electrochemical activity in aqueous electrolyte, but was not tested in a Mg non-aqueous electrolyte.^[161] The structure of the magnesium manganese oxide spinel $MgMn_2O_4$ is different compared to the typical cubic structure of other spinels, mainly due to the Jahn-Teller effect of Mn^{3+} . It is a partially inverted spinel with a majority of $Mn(III)$ in the octahedral sites as well as a fraction of $Mn(IV)$ and $Mn(II)$ in the octahedral and tetrahedral sites.^[162] Despite the sluggish diffusion of Mg^{2+} into the tetragonal spinel, experiments revealed that the delithiated cubic phase λ - Mn_2O_4 can insert Mg^{2+} in aqueous and non-aqueous electrolyte.^[103,162] However, the insertion drives a phase transformation from cubic Mn_2O_4 to tetragonal $MgMn_2O_4$, which may be one reason for the low magnesiation degree (3 wt% Mg in the discharged state for non-aqueous electrolyte).^[163] That differs from the insertion of Li, which is only using the cubic phase. Tetragonal $MgMn_2O_4$ (MMO_T) is a partially inverted spinel with distorted oxygen octahedra, due to $Mn(III)$ which induces the Jahn-Teller distortion. In that case, the Mn^{3+} and Mg^{2+} exchange positions due to their similar ionic radii (0.63 Å for tetrahedral Mg^{2+} and 0.72 Å for Mn^{3+}) and Mn^{3+} occupies the octahedral side while Mg^{2+} occupies the tetrahedral site.

Compared to the MMO_T, the cubic $MgMn_2O_4$ (MMO_C) is a highly inverted spinel (λ -0.45) in which $Mn(IV)$ ions replace the $Mn(III)$ Jahn-Teller active ions at the octahedral sites, while the remaining $Mn(II)$ ions are located in the tetrahedral sites. Mg^{2+} is located in the tetrahedral and the octahedral sites. The structural differences are well known for MMO_T and MMO_C, however, the mechanism of Mg^{2+} diffusion in the cubic structure is not well understood. The comparison between MMO_T and MMO_C was also investigated experimentally in a coin cell set-up by using $Mg(TFSI)_2$ /PC electrolyte.^[162] The CV profiles in Figure 17a reveal that the electrochemical current is

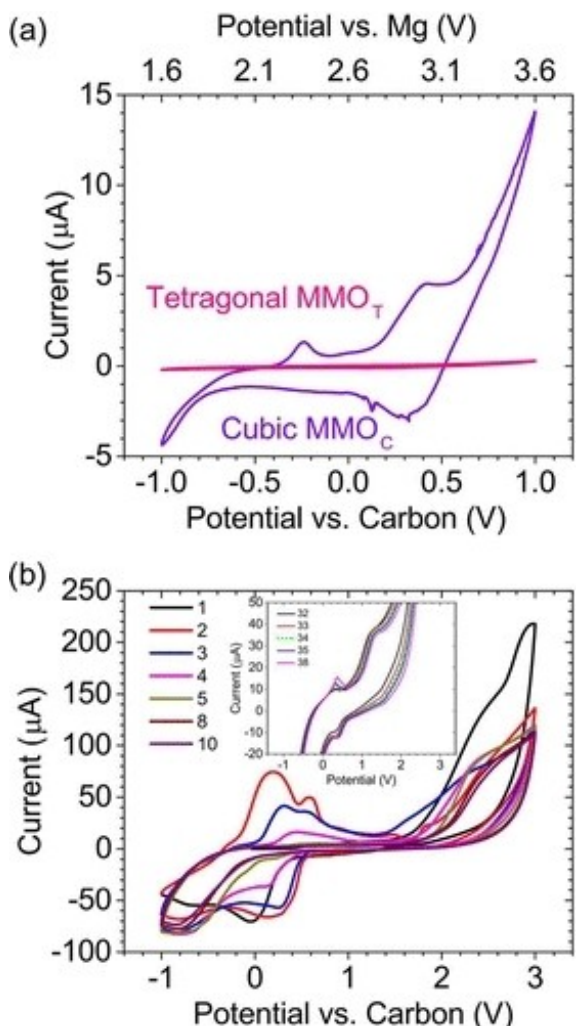


Figure 17. a) Cyclic voltammetry (CV) of tetragonal MMO_T (pink) and cubic MMO_C (purple) thin film coin cells at 1 mV s⁻¹ scan rate with BP2000 carbon on stainless steel as the anode and with 0.2 M Mg(TFSI)₂ in PC as the electrolyte. The bottom axis is the measured voltage versus carbon, and the top axis is the estimated Mg/Mg²⁺ voltage. The carbon voltage was converted to Mg/Mg²⁺ voltage by measuring its open circuit voltage versus a Ca reference electrode, which was calibrated in the same electrolyte using the ferrocene couple. (b) CV data for cycling tests of the MMOC at 1 mV s⁻¹ scan rate. The redox peaks gradually decrease indicating capacity fade, but the redox peaks are still visible after 38 cycles. Reprinted from Ref. [162] with permission. Copyright (2015) American Chemical Society.

rather small, whereas MMO_C reveals a substantial redox activity with an estimated charge capacity of 250 mAh g⁻¹ in the 2nd cycle (270 mAh g⁻¹ theoretical value). However, the redox peaks gradually faded with increasing cycle number. This fast capacity fading and the low coulombic efficiencies were assigned to the degradation of the thin film.

Additionally, it is worth mentioning that the crystallite size has a significant influence on the electrochemical performance for Mg (de)insertion into the MgMn₂O₄ structure. Two different crystallite sizes (11 nm (MMO-1) versus 31 nm (MMO-2)), were tested in both anhydrous (0.5 M Mg(TFSI)₂ in ACN/0.5 M dipropylene glycol dimethyl ether) and hydrated electrolyte (0.5 M Mg(TFSI)₂ + 3 M H₂O in ACN/0.5 M dipropylene glycol dimethyl ether) (See Figure 18).

Comparing the CV of both electrodes, the MMO-1 shows in anhydrous electrolyte 4 times higher peak current than MMO-2, and in the hydrated electrolyte 3 times higher peak current.^[164]

Since sulfides like Li_xTiS₂ are known to exhibit good kinetics and good cycle life as cathode materials for in Li-ion batteries, it serves as a useful model to explore the properties of Mg intercalation into spinel (and layered) crystal structures.^[165] Since sulfur spinels have a soft anion lattice, which leads to weaker coulombic attraction between guest Mg²⁺ and host structure, sulfur-based spinels exhibit higher Mg²⁺ mobility and quite good cycle life compared to oxide spinels.^[165–168] Another big advantage of sulfides is the absence of unwanted phase transformations during the Mg/Li insertion and removal. Transition metals oxides, in contrast, are more ionic which make them more prone to polarization issues, disorder/order structural variations and additional conversion reactions.^[165,169] Sulphur spinels have the general formula AB₂S₄ (Fd3m space group), in which the A atoms are Mg, Ca or Zn and the B atoms, as redox-active 3d transition metals, are Ti, V, Cr, Mn, Fe, Co, Ni.^[159] Thiospinels are arranged so that each transition metal is octahedrally coordinated by an S atom with a large space in between for fast ion diffusion.^[160]

Similarly to the oxide spinels, in sulfide and selenide spinels, ion migration between two tetrahedral sites (*tet*) occurs via a vacant octahedral site (*oct*), which shares a face with the tetrahedral sites, following the migration topology *tet-oct-tet* (Figure 19a). The magnitude of the migration barrier depends highly on the size of the triangular face (Figure 19b) between *oct* and *tet* sites, and by the anionic species that form the triangle.^[170]

There are two highly symmetric sites in spinel structures that can accommodate Mg²⁺ ions: *oct* and *tet* sites. The size and electronic structure of sulfide spinel hosts affect the multivalent intercalant site preference. Figure 20b suggests that, i.e. in Mn based spinels, the Mg is stable in both sites (*oct* and *tet*). By looking at the thermodynamic stability of different compounds of the thiospinel family, and comparing their formation energy against the convex hull of ground state energies in the relevant portion of the phase diagram, a smaller energy above the hull suggests that the material is more likely to be stable and can be synthesized.

Figure 20 suggests that Ti₂S₄ and Mn₂S₄ spinel structures exhibit the most stable host material compared to V, Cr, Ni, Co, and Fe containing host materials for cation intercalation. Since the ionic radius of Mg²⁺ is relatively small compared to Ca²⁺, tetrahedral and octahedral environments are both favored. Computational calculations showed that the radius ratio for sulfides is 0.391 and for selenides 0.364, suggesting a preference to larger tetrahedral or smaller octahedral environments for Mg²⁺.^[171] (See Figure 21).

Compared to Mg²⁺, the larger Ca²⁺ ion prefers the rock salt type structure, which are octahedrally coordinated. Liu et al. further investigated the diffusion activation barriers by using nudged-elastic band (NEB) calculations. Compounds with reasonable cation mobilities (Table 4) include Mg in Mn₂S₄ (515 meV), Mg in Cr₂S₄ (567 meV) and Mg in Ti₂S₄ (615 meV). The table also reveal that the diffusion barrier can be lowered

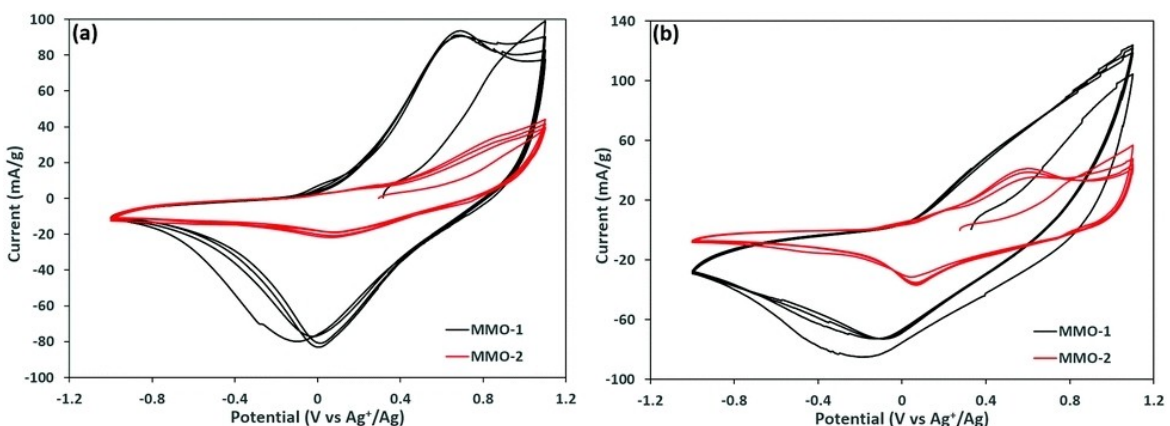


Figure 18. Cyclic voltammetry test of MMO-1 (11 nm) and MMO-2 (31 nm) in a) 0.5 M $\text{Mg}(\text{TFSI})_2$ in acetonitrile/0.5 M dipropylene glycol dimethyl ether, b) 0.5 M $\text{Mg}(\text{TFSI})_2 + 3 \text{ M H}_2\text{O}$ in acetonitrile/0.5 M dipropylene glycol dimethyl ether electrolyte. Scan rate: 0.1 mV s^{-1} . Reprinted from Ref. [164] with permission. Copyright (2017) Royal Society of Chemistry.

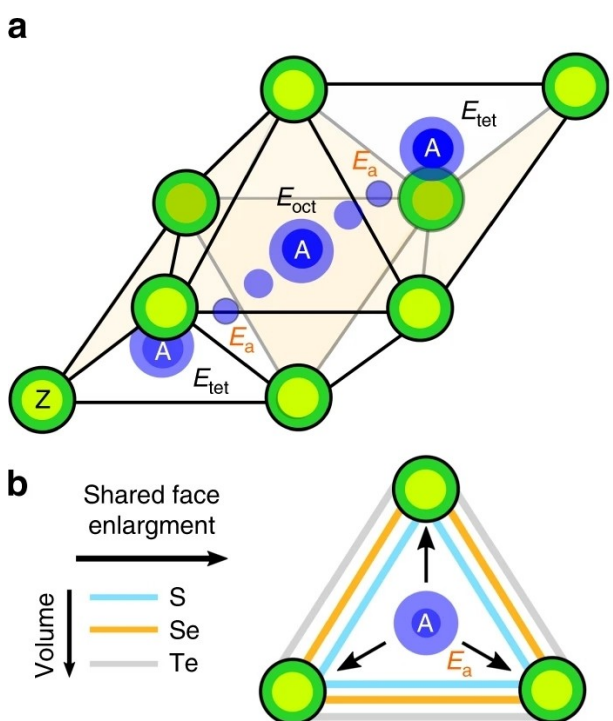


Figure 19. First-principles Mg and Zn migration barriers in sulfides, selenides, and tellurides AX_2Z_4 spinels (with A=Mg or Zn); tet–oct–tet migration path in the AX_2Z_4 framework, with energy of the tet, oct, and transition sites indicated by E_{tet} , E_{oct} , E_{a} , respectively. E corresponds to the migration energy. Reprinted from Ref. [170] under the terms of the Creative Commons CC BY License. Copyright (2017) The Authors.

by using Mn, Ni or Cr based spinels, instead of Ti based spinels. Additionally, NiS_2 (0.46 eV) show comparable activation barrier for Mg diffusion to those for Li diffusion in LiTi_2O_4 (0.56 eV).^[159,169] Electrochemical investigations (Figure 22a) were carried out for a cubic Ti_2S_4 spinel cathode vs. Mg metal anode in $(\text{PhMgCl-AlCl}_3)/\text{G4}$ (APC-electrolyte) with an initial discharge capacity of 200 mAh g^{-1} at 60°C (C/20). The sloping curve between $1.50 \text{ V}-1.00 \text{ V}$ (Mg CE-2 Electrode Setup) demonstrates a solid-solution Mg^{2+} insertion mechanism. From cycle 2, the capacity drops (Figure 22b) to about 140 mAh g^{-1} which is attained till 40 cycles at a C-rate of C/10. It was also reported that the capacity fading might be due to micron-sized active material particles, which could trap the Mg^{2+} during charge.^[168]

Although the calculations for the sulfide spinels seem to be advantageous compared to oxides in terms of diffusivity, thiospinels operate at lower potentials and shows lower specific capacities.^[159]

In summary, neither Mn oxides nor Ti/Mn sulfides exhibit both good Mg ion mobility and high specific capacities. It might be reasonable to look for different strategies, to find suitable host materials for the insertion/intercalation of Mg^{2+} . One suggestion could be the use of known stable host materials of Na ion batteries and try to exchange Na with Mg. First theoretical calculations by Hannah et al. reveal for a $\text{V}_{1.25}\text{Ti}_{0.75}\text{O}_4$ host structure (desodiated state) an excellent Mg mobility ($< 300 \text{ meV}$) and an average insertion potential for Mg of 1.50 V (vs Mg/Mg^{2+}) considering a theoretical capacity in the range of $281-285 \text{ mAh g}^{-1}$ which would be higher than state of the art thiospinel cathodes. In case the empty structure can be

Table 4. Properties of selected multivalent sulfur spinel systems. Adapted from Ref. [159] with permission. Copyright (2016) Royal Society of Chemistry.

Spinel materials	Stable "A" site	Voltage [V]	Capacity [mAh g^{-1}]	Diffusion barrier [meV]
Mg in Cr_2S_4	tet	1.65	209	542
Mg in Ti_2S_4	oct	0.89	216	615
Mg in Mn_2S_4	oct	1.00	204	515
Ca in Cr_2S_4	oct	2.16	197	567

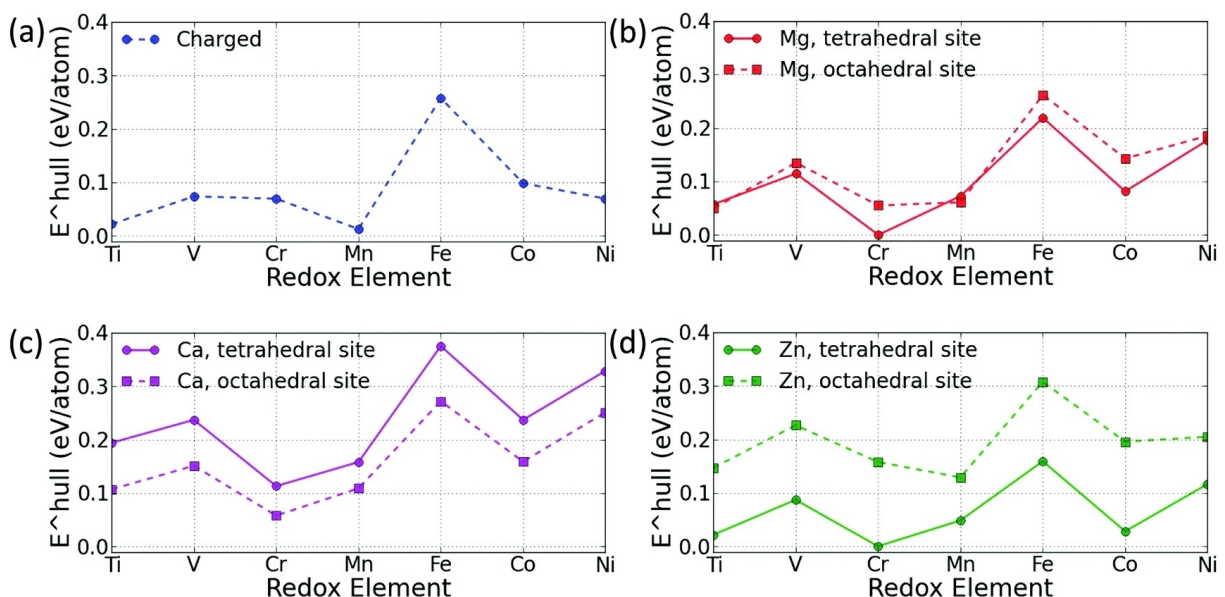


Figure 20. The calculated thermodynamic stabilities of sulfur spinel compounds in the (a) charged and (b–d) discharged phases. The energy above hull is measured as the formation energy difference between a compound and the convex hull formed by stable compounds. The distance between the dashed and solid lines indicate site energy preferences for the cation in the discharged state. Reprinted from Ref. [159] with permission. Copyright (2016) Royal Society of Chemistry.

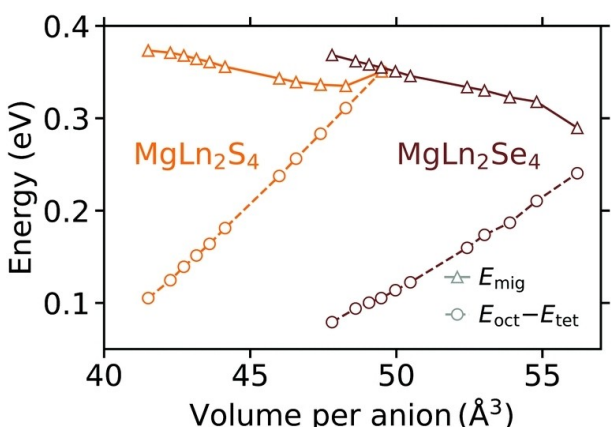


Figure 21. Comparing the Mg^{2+} migration energy, E_{mig} , to the difference in octahedral and tetrahedral energies, $E_{oct} - E_{tet}$ as a function of the calculated volume per anion in the pristine structures. Reprinted from Ref. [171] with permission. Copyright (2020) Royal Society of Chemistry.

obtained via desodiation, the host material seems to be as stable as the 50% magnesiated structure. DFT calculation revealed a thermodynamic driving force for decomposition especially at the fully magnesiated phase.^[172] Recently, the group of Sun et al. used the $NaV_{1.25}Ti_{0.75}O_4$ cathode material and applied those theoretical calculations. They extracted sodium chemically and electrochemically and electrochemically intercalated Mg^{2+} ions, with a Mg anode and 0.5 M $Mg(CB_{11}H_{12})_2$ in tetraglyme electrolyte at 5 mA g⁻¹ current density and 60 °C. The chemically desodiated material ($Na_{0.25}V_{1.25}Ti_{0.75}O_4$) shows at an average voltage of 1.50 V (Mg CE-2 Electrode Setup) with an initial sloping potential up to 50 mAh g⁻¹ specific capacity, followed by a steeper profile until it reaches 80 mAh g⁻¹ at the end of discharge.

The following charge only retrieves half the initial capacity together with a large overpotential, as can be seen in Figure 23. The low electrochemistry performance was addressed to amorphization happening during the Na extraction. The electrochemically desodiated material ($Na_{0.4}V_{1.25}Ti_{0.75}O_4$) exhibits poorer Mg^{2+} intercalation. However this might be due to the higher Na content. The difficulties in inserting Mg^{2+} cations into the structure was also mainly addressed to structural degradation which is also in good agreement with the theoretical investigations. Nevertheless, although there are several difficulties which need to be overcome it might be a future strategy to adopt cathode host structures of Li and Na ion batteries to divalent insertion/intercalation.^[48]

5. Calcium Cathode Materials

Obviously, Ca and Mg chemistries are sharing some similarities (divalent cations and close potentials vs. SHE) which suggests a similar chemistry and electrochemistry. Moreover Ca^{2+} and Na^+ share a similar ionic radius (ionic radii in metal oxides: $r(Ca^{2+})VI = 1.0 \text{ \AA}$ and $r(Na^+)VI = 1.02 \text{ \AA}$)^[173] pointing out potential similarities for preferential intercalation sites. However, each metal is unique and exhibits a unique chemistry. Electrochemical intercalation of Ca^{2+} for positive electrode materials was firstly published in the early 2000s using a Prussian blue based cathode hexacyanoferrate in an aqueous electrolyte^[174] or V_2O_5 and $Ca(ClO_4)_2$ in an ACN-based electrolyte.^[175]

As for a Mg cathodes, introducing water into non-aqueous electrolytes enhances the electrochemical reversibility of Ca intercalation/extraction, even if its role is not fully elucidated.^[176] The quest for cathode materials to intercalate

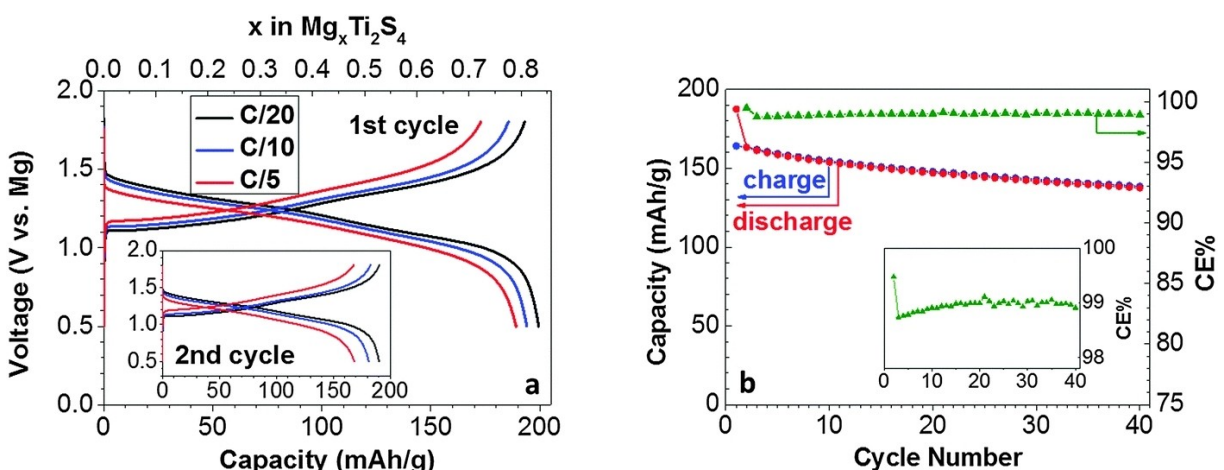


Figure 22. Electrochemistry of C-Ti₂S₄ coin cells with an APC electrolyte and a Mg negative electrode at 60 °C. a) Discharge and charge curves of the first and second (inset) cycles at various rates in APC/THF electrolyte. b) Capacity and coulombic efficiency (CE) evolution at a C/10 rate in APC/G4 electrolyte (inset showing 99% CE). Reprinted from Ref. [168] with permission. Copyright (2016) Royal Society of Chemistry.

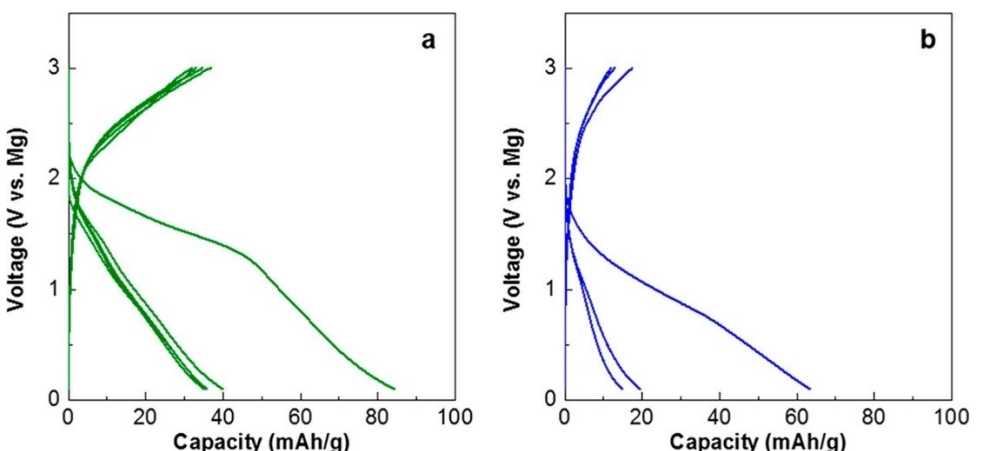


Figure 23. Electrochemistry of a) chem-ox-2 and b) electrochemically desodiated material (i.e., Na_{0.4}V_{1.25}Ti_{0.75}O₄) with a Mg anode and 0.5 M Mg(CG₁₁H₁₂)₂ in tetraglyme electrolyte at 5 mA g⁻¹ current density and 60 °C. Reprinted from Ref. [48] with permission. Copyright (2018) American Chemical Society.

Ca²⁺ is challenging. Computational studies predicting low migration barriers for some cathode materials show that the choice of a Ca cathode material is not straightforward since, in contrast with those studies, most materials are not able of inserting/extracting Ca²⁺ cations experimentally.^[37,38,77] A direct transfer of knowledge from LIBs or SIBs into Ca systems seems not possible. Additionally, reliable electrochemical tools to assess the Ca system are not up to date and accessible, thus making difficult the metrics evaluation of Ca batteries.

To date, the Ca²⁺ intercalation chemistry in a variety of potential host cathode candidates, such as spinels, Prussian Blue Analogues, Polyanionic structures or V₂O₅ layered oxides, has been investigated.

DFT calculations, as shown in Figure 24, predicted the existence of CaMn₂O₄ with Ca²⁺ in the tetrahedral sites, which seems to be practically impossible.^[179,180] Only marokite CaMn₂O₄ seems to be stable, with Ca²⁺ cations in octahedral sites.^[179] Furthermore crystal structures with Ca²⁺ in tetrahedral sites for halides, chalcogenides^[21] or oxides are not listed in the

Inorganic Crystal Structure Database (ICSD).^[173] Regarding stable Ca-olivine type structures, they exist in the mineral kirschsteinite CaFeSiO₄,^[181] and the larger Ca²⁺ occupies the M2 site being thus immobile.^[177] As in the olivine LiFePO₄, with its hexagonal close packing array of oxygen atoms, two different octahedral sites M1 and M2 are present (see Figure 25). M2 site provides a suitable channel for Ca²⁺ diffusion and intercalation.^[144,182] The M1 octahedral site is comparatively more distorted and smaller, whereas the M2 site is more regular and larger. Ca²⁺ can be also intercalated in some ordered rock-salt structures such as nanoclusters of CaMnO₂^[183] and layered-Ca_{0.47}CoO₂.^[184]

As layered oxides, common host materials such as V₂O₅, MoO₃, and TiS₂, have been identified as potential candidates to intercalate Ca²⁺ especially V₂O₅.^[175,185,186] Layered vanadium V₂O₅ is an effective host material for the intercalation of alkali metals with a rather high charge/discharge rate. Moreover, layered structures favor intercalation reactions and the appealing high redox potential of the V⁵⁺/V⁴⁺ couple made V₂O₅ one

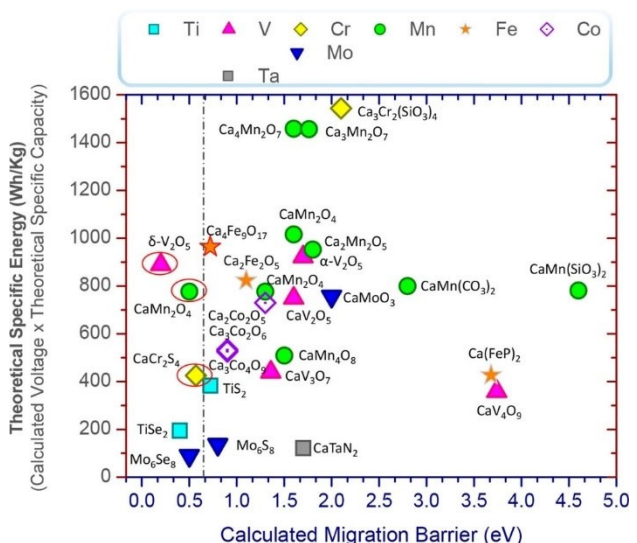


Figure 24. Theoretical specific energy vs calculated energy barriers (eV) for proposed Ca hosting TM compounds. The specific energy is estimated from the calculated average voltage for a particular redox couple and the corresponding theoretical specific capacity. The vertical line denotes the criterion for good cathode performance (<0.650 eV, see text). Reprinted from Ref. [43] with permission. Copyright (2019) American Chemical Society.

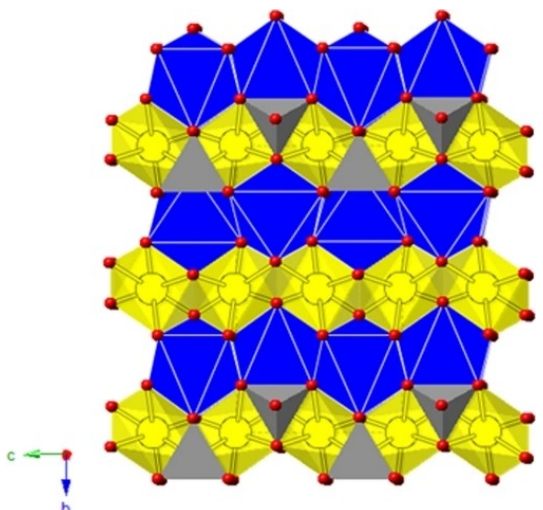


Figure 25. View of the olivine structure showing the octahedral M1 (in yellow) and M2 (in blue) sites, and tetrahedral Si (in grey). The M1 sites form channels for cation diffusion. Reprinted from Ref. [177] under the terms of the Creative Commons CC BY License. Copyright (2019) The Authors.

of the first materials tested for Ca intercalation. In previous works Li intercalation was already investigated into V_2O_5 and exhibited a reversible capacity of 130 mAh g^{-1} for microcrystalline V_2O_5 .^[187]

For Mg^{2+} and Ca^{2+} intercalation, the reversible capacity was increased to 180 mAh g^{-1} and 200 mAh g^{-1} .^[56,186] Wang et al. investigated the structural stability, intercalation potentials and rate capability of Na^+/Ca^{2+} intercalation into α - and δ - V_2O_5 by using DFT calculations (see Figure 26).^[178] The major difference between α - V_2O_5 (space group Pmm) and δ -phase (space group of $Cmcm$) is the shift of α - V_2O_5 layers in 100

direction by $a/2$. The crystal structure of V_2O_5 is build up as layered V_2O_5 pyramids connected by a bridging oxygen. The location of the Na^+/Ca^{2+} ions in both structures ($\alpha + \beta$) is in the middle of the V_2O_5 pyramid (along 100 plane) and between two layers. However, the α - V_2O_5 and α - CaV_2O_5 seem to be more stable than the equivalent δ -structures. Nevertheless the Ca^{2+} diffusion barrier is lower in the delta δ - V_2O_5 (0.74 eV) and δ - CaV_2O_5 (1.39 eV) respectively, compared to the α - V_2O_5 (0.98 eV) and α - CaV_2O_5 (1.83 eV),^[178] respectively. Wang et al. also compared the theoretical insertion potentials in α - and β - V_2O_5 for Ca^{2+} insertion with Na^+ insertion. It was also found that the average theoretical intercalation potentials for Na^+ in α - V_2O_5 was ~ 2.60 V for $0 < x < 1$ whereas the δ - V_2O_5 phase was not accessible during the intercalation process.^[178]

Depending on the energy required to expand the interlayer space, ions are intercalated more favorably into a single layer until the maximum capacity (stage I). In case all layers are filled, the intercalation process is called stage II.^[178] The high voltages of the intercalation of Na^+ and Ca^{2+} into α - V_2O_5 to $Na_{0.167}V_2O_5$ and $Ca_{0.33}V_2O_5$ lead to the conclusion that the ions intercalate based on stage I, whereas the lower voltages of $Na_{0.333}V_2O_5$ to $Na_{0.661}V_2O_5$ as well as $Ca_{0.333}V_2O_5$ to $Ca_{0.661}V_2O_5$ are based on stage II.^[178] Another classical material in intercalation chemistry is TiS_2 with potential to reversibly intercalate Ca^{2+} ions.^[34,188] Recent DFT investigations indicated a distinct site preference of the intercalant ions.^[189] Thus, Mg^{2+} and Li^+ occupy the empty octahedral sites in the interlayer space of the initial O1 lattice (CdI_2 -type structure), forming stage compounds as intercalation proceeds. In contrast, the large intercalants Na^+ , K^+ , and Ca^{2+} occupy the prismatic sites in a P3 stacking at intermediate concentrations ($x \approx 0.5$) with minimized in-plane electrostatic repulsions.^[180,181]

Prussian blue analogues (PBAs) have the general formula $A_xMM'(\text{CN})_6 \cdot nH_2O$ in which A is an alkali or alkaline-earth metal, M and M' a transition metal and $-(\text{CN})-$ is a chemical bond in the corner-shared octahedral.^[67] (See Figure 27). It seems to be an attractive cathode material due to its high specific capacity, nontoxicity, low cost and simple synthesis. $NiFe(\text{CN})_6$ and $CoFe(\text{CN})_6$ have been investigated as intercalation cathode materials for RCBs with capacities of 50 mAh g^{-1} and 82 mAh g^{-1} and good capacity retention in water-containing electrolytes.^[190] However, it is also well known, that aqueous systems are not compatible with Ca-metal anodes. The group of Ling et al. investigated the crystal structure with DFT calculations.

Iron hexacyanoferrate has a cubic crystalline framework with the space group $Fm\bar{3}m$ in which Fe ions are located at the corners of the cube connected by cyanide ligands.^[191] Fe ions show an octahedral coordination and are bonded to carbon or to nitrogen. In a strong crystal field, the carbon coordinated Fe is present in a low-spin configuration, whereas the nitrogen coordinated Fe in a weak crystal field prefers a high spin configuration. The oxidation state of Fe ions in stoichiometric $Fe[\text{Fe}(\text{CN})_6]$ with no interstitial cation is Fe^{3+} . During intercalation of cations, either alkali or alkaline earth cation, Fe^{3+} is reduced to Fe^{2+} . The crystal structure of FeHCF provides large empty spaces for the intercalation of cations or even small molecules. DFT calculations show an optimized lattice parame-

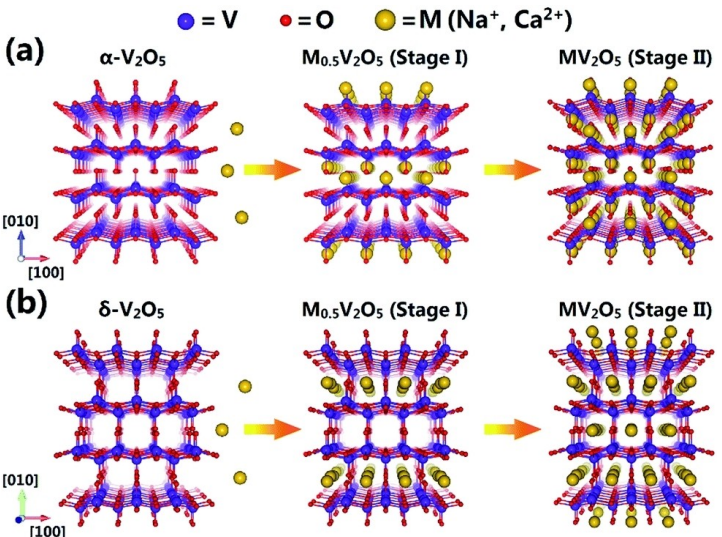


Figure 26. Schematic illustration of the stage I and stage II arrangements of Na/Ca storage in a) α - V_2O_5 and b) δ - V_2O_5 . Reprinted from Ref. [178] with permission. Copyright (2016) Royal Society Of Chemistry.

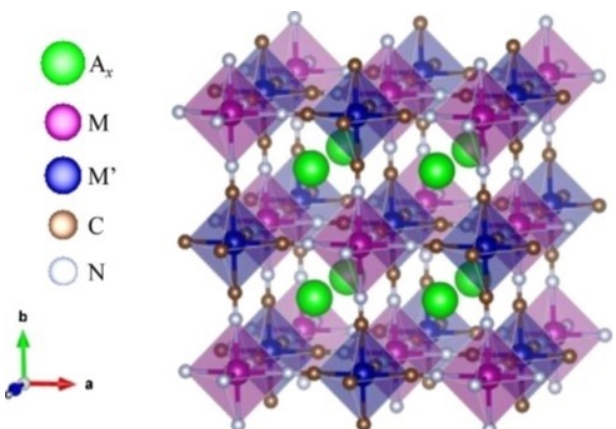


Figure 27. Crystal structure of PBAs with the A_x represented in light green, the M and M' transition metal represented in violet and blue, the C and N presented in brown and silver at the corner-shared octahedral. Reprinted from Ref. [67] with permission. Copyright (2016) Elsevier.

ter of 10.14 \AA , which is in good agreement with the experimental reports of 10.178 \AA .^[191]

There are several possibilities of locating a cation in the interstitial sites in the cubic structure. In accordance with the Wyckoff notations, they can be described as 8c (body centered), 24d (face-centered), 32f (displaced from 8c sites towards N coordinated corner), 32f' (displaced from 8c sites towards C coordinated corner) and 48g (displaced from 8c and 24d). The alkali ion Na^+ as well as the alkali earth metals Mg^{2+} and Ca^{2+} prefer to occupy the 24d sites while in comparison the Li^+ ion prefers the 48g site^[192] (See Figure 28).

Lipson et al. investigated the Ca-ion intercalation by desodiating a $Na_xMnFe(CN)_6$ (MFCN) structure galvanostatically, versus a carbon anode in 1 M $NaPF_6$ in 3:7 EC:EMC electrolyte. Afterwards the electrode was cycled in a nonaqueous 0.2 M $Ca(PF_6)_2$ electrolyte using the same cell geometry.^[68] The carbon-based electrode was used because the metallic Ca

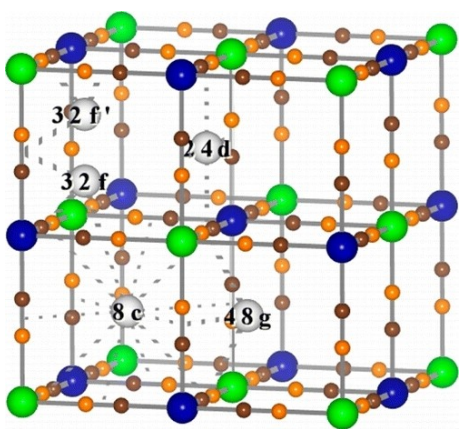


Figure 28. Crystal structure of iron hexacyanoferrate ($Fe[Fe(CN)_6]$) and possible interstitial sites (white color). Blue, high-spin Fe; green, low-spin Fe; brown, nitrogen; orange, carbon. Reprinted from Ref. [192] with permission. Copyright (2013) American Chemical Society.

metal anode cannot be reversibly cycled with high coulombic efficiency.

In Figure 29 the galvanostatic charge-discharge curves of MFCN in sodium-based electrolyte and Ca-based electrolyte are presented. The capacity approaches the theoretical capacity of 183 mAh g^{-1} for $Na_{11}MnFe(CN)_6$, assuming two sodium atoms can intercalate per formula unit, which is supported by two distinct plateaus indicating that both the Fe and Mn are changing oxidation state during cycling.^[69] In comparison with the Na system, the desodiated MFCN in Ca-based electrolyte show only one plateau indicating that only one transition metal is reduced when Ca is inserted. These results show that Ca^{2+} reversibly intercalate into MFCN in a dry non-aqueous electrolyte with a capacity of 80 mAh g^{-1} . It was reported that at a potential of 3.4 V vs Ca/Ca^{2+} (Carbon CE), only Mn oxidizes, which implies a theoretical capacity of 100 mAh g^{-1} .^[68]

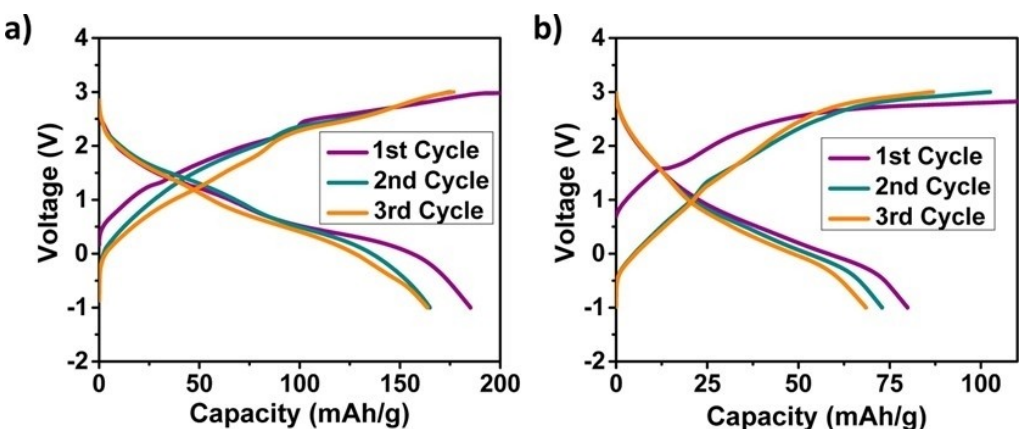


Figure 29. Galvanostatic charge-discharge curves of a) MFCN in 1 M NaPF_6 in a 3:7 EC:EMC electrolyte and b) desodiated MFCN in 0.2 M $\text{Ca}(\text{PF}_6)_2$ in a 3:7 EC:PC electrolyte using a BP2000 carbon anode and a rate of 10 mA/g. Reproduced from Ref. [68] with permission. Copyright (2015) American Chemical Society.

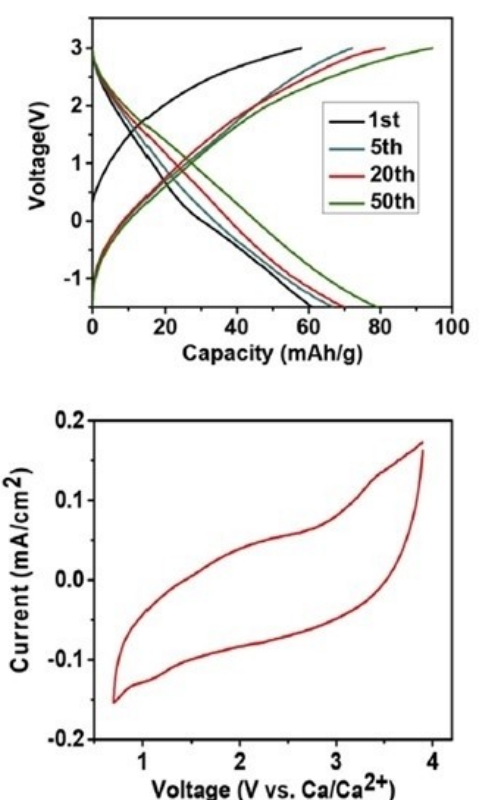


Figure 30. a) Voltage profiles from galvanostatic cycling of a coin cell at a rate of 10 mA/g and b) cyclic voltammetry taken at 1 mV s⁻¹ for desodiated $\text{Na}_2\text{FePO}_4\text{F}$ using a 3-electrode cell. Reprinted from Ref. [69] with permission. Copyright (2017) Elsevier.

Other polyanions frameworks such as phosphates, vanadates and NASICON, used to intercalate Na^+ and Li^+ ions, have also been recognized as potential candidates for Ca^{2+} intercalation.^[193] The iron fluorophosphate ($\text{A}_2\text{FePO}_4\text{F}$) has been already successfully used as an intercalation material for Sodium and Lithium. Fluorophosphates, which seem to be potential high voltage cathode materials, combine the inductive effect of the PO_4^{3-} group and the high electronegativity of

the F^- anion to enable fast Ca^{2+} insertion.^[193] Iron phosphate is prepared in its reduced form in order to allow using it directly as a positive electrode. The crystallized structure has a $Pbcn$ orthorhombic space group. The bi-octahedral $\text{Fe}_2\text{O}_7\text{F}_2$ units which contains face sharing FeO_4F_2 octahedra, are forming chains with bridging F atoms and together with tetrahedral PO_4 units, infinite FePO_4F units are formed.^[193] The two Na^+ ions are located in the interlayer space, which undergoes facile two dimension migration pathways due to the limited transport in the third dimension.

Differing from LiFePO_4 a sloping potential from $\text{Na}_2\text{FePO}_4\text{F}$ was observed which indicates a quasi-solid solution electrochemical behavior. Upon oxidation of the $\text{Na}_2\text{FePO}_4\text{F}$, a small change (~4%) of the crystal unit volume suggests a lower de-/intercalation strain. Since the ionic radii of Na^+ and Ca^{2+} are similar, Ca^{2+} intercalation seems to be possible into the Na-host material. The group of Lipson investigated Ca^{2+} intercalation into a desodiated $\text{Na}_2\text{FePO}_4\text{F}$ cathode in a non-aqueous electrolyte [0.2 M $\text{Ca}(\text{PF}_6)_2$ in 3:7 EC:PC]. After sodium was removed electrochemically, the electrode was rinsed and cycled versus a carbon capacitive counter electrode. The electrochemical measurements suggested that Ca^{2+} was successfully intercalated into desodiated $\text{Na}_2\text{FePO}_4\text{F}$ with a potential of 2.600 V (vs. Ca/Ca^{2+}) and a capacity of 80 mAh g⁻¹ (Figure 30).^[69] The intercalation mechanism was similar to that of sodium with the appearance of an intermediate half-filled phase (e.g. $\text{Na}_{1.5}\text{FePO}_4\text{F}$ or $\text{Ca}_{0.25}\text{NaFePO}_4\text{F}$).

Recently, Kim et. al.^[62] reported the synthesis and electrochemical investigations on desodiated $\text{NaV}_2(\text{PO}_4)_3$ and delithiated LiFePO_4 materials, focusing on Ca cation insertion/extraction at room temperature. The authors reported a reversible capacity of around 81 mAh g⁻¹ at 3.2 V (vs. Ca/Ca^{2+}) average potential for 40 galvanostatic cycles. The measurements were carried out in a 3-electrode setup using activated carbon as counter electrode, which was calibrated vs. Ca/Ca^{2+} comparing its potential with delithiation potential of LiFePO_4 in different cells. On the other hand the FePO_4 framework exhibited a higher first cycle discharge capacity of 103 mAh g⁻¹ with a 2.9 V (vs. Ca/Ca^{2+}) working potential. The olivine

framework showed marked capacity fade with respect to the NASICON phase. Insertion/extraction processes were confirmed via a combination of different spectroscopic techniques showing a non-uniform insertion of divalent Ca cations from a surface-to-bulk point of view.

Liu et al. investigated the theoretical performance of the spinel structure host with the general formula AB_2O_4 ($A=Al, Y, Mg, Ca, Zn$ and $B=Ti, V, Cr, Mn, Fe, Co, Ni$) for multivalent battery application.^[159] The spinel structure has a space group of Fd3m. Outgoing from AB_2O_4 the A ion occupies the tetrahedral sites whereas the B ion occupies the octahedral sites, coordinated by oxygen. The B atoms form a network with empty sites interconnecting in 3 dimensions.^[159] Previous studies already showed the successful ion exchange in $LiMn_2O_4$ of Li^+ with Mg^{2+} and exhibited reversible intercalation and deintercalation. Compared to Li^+ intercalation, the Ca^{2+} insertion should occur according to Liu et al. at a 0.7 V lower value.^[37] Nevertheless, the Ca spinel structure is thermodynamically less stable when compared to the Mg system. Additionally, the volume expansion for divalent ions such as Ca^{2+} is significantly larger (up to 30%) compared to Li^+ and Mg^{2+} which is up to 10%.^[37]

Arroyo et al. investigated with DFT calculations perovskite $CaMoO_3$ which combines good electronic conductivity, moderate crystal structure modifications, activity in the 2.00–3.00 V (vs Ca/Ca^{2+}) region and several intermediate Ca_xMoO_3 stable phases.^[38] The Ca ion mobility was investigated by constructing $Ca_{15}Mo_{16}O_{48}$ supercells with lattice parameter $a=11.2\text{ \AA}$, $b=7.8\text{ \AA}$, and $c=10.9\text{ \AA}$ in which the minimum distance for Ca^{2+} vacant sites is 7.8 Å. However, in the orthorhombic system the Ca mobility is hindered with barriers exceeding 2 eV. In general, Ca^{2+} deinsertion from orthorhombic $CaMoO_3$ perovskite would occur at an average potential of about 3.50 V (vs Ca/Ca^{2+}). However, with experimental analysis it was not possible to detect Ca deinsertion and based on DFT results the lack of deinsertion is ascribed to low Ca^{2+} diffusivity in perovskite structure.^[38]

6. Cell setup And Data Reporting

Research on multivalent-ion batteries (MIBs) presents several hurdles and obstacles that can make the path to a complete understanding challenging, if not very difficult. Among those, reproducible and detailed procedures for experiments and data acquisition, as well as data reporting, are often overlooked, potentially leading to an incorrect interpretation of the obtained results.

The need for reliable electrochemical setups is a non-negotiable requirement in order to obtain consistent data and all the involved elements, from cell setup to a proper choice of counter (CE) and/or reference electrodes (RE), needs utmost care. Unfortunately, these details cannot be always retrieved by the final reader of a scientific paper. For this reason, an approach that starts from the readers' perspective could be a good starting point to reflect on the matter.

Often, in the multivalent-ion battery research field, the lack of experimental details on the used conditions and the overlooking of known aspects—e.g., electrolyte decomposition at certain potentials—can lead to misinterpretation of results. One first critical point is about the experimental sections of published papers, which are the core for the correct evaluation of data, and these sections are often lacking important details, like the use of non-conventional pseudo reference electrodes or the used experimental conditions.

Speaking of pseudo-REs, operating in non-aqueous environments complicates the working conditions, and finding an appropriate one, ensuring non-polarizability, reproducibility, and stable potentials in different temperature conditions can be a challenging task.^[194] While for other established chemistries, like LIBs,^[195] or more studied but still out-of-market systems like SIBs more is known about the metal electrode behavior as pseudo reference, Mg (−2.37 V vs. SHE) and Ca metal (−2.87 V vs. SHE) still present considerable stability issues and different behaviors depending on the electrolyte system of choice. The sensitivity and high reactivity of the alkaline-earth metals with the working environment can be an important source of variability to be considered in the relative stability of the Mg/Ca QREs.

In this regard, a solid and reliable way to evaluate and address the stability issue is the use of an internal standard like the ferrocene/ferrocenium (Fc/Fc⁺) couple to carry out a calibration experiment, by means of Cyclic Voltammetry (CV). In this regard, it must be stressed, that while several papers report the use of alternative pseudo-REs, almost no author reports detailed data about the actual calibration and/or stability tests, leaving the final reader in the dark about potential shifts over time. A possibility, already explored in scientific literature, is the implementation of Activated Carbon (AC) as candidate material.^[196] It is known that AC CEs are influenced not only by the salt of choice, but also the chosen solvent, as reported in literature.^[197] Among the most used salts there are $Mg(TFSI)_2$, $Mg(ClO_4)_2$, $Mg(BH_4)_2$, $Ca(TFSI)_2$, $Ca(BH_4)_2$, $Ca(BF_4)_2$ in acetonitrile (ACN), Propylene Carbonate (PC), 1,2-Dimethylethoxyether (DME) and glymes. Since more and more often these electrolyte systems are reported in different concentrations, it is not hard to understand how variable the conditions are and how sensible the collected data could be. This evidences that a careful calibration of the system should be performed in each different case. This is a not negligible detail to have a full understanding of the presented experiments. This aspect is especially important for the wide variety of alternative pseudo-REs used in post-Li literature papers, like Ag/AgCl and AC. In particular, in the case of AC pseudo-REs and CEs, a detailed preparation procedure of the actual electrodes should be reported.

Experimental details have to be supported by means of detailed calibration curves, the time-dependent voltage shift and an exemplary of cycling profile of activated carbon as CE. The stability region of electrolyte should be also reported for a better interpretation of the graphical data since it is well known that the solid electrolyte interface it is a barrier for Mg^{2+} and

Ca^{2+} cation diffusion, and during electrolyte degradation a cathode solid electrolyte interface could be also generate.

Concerning counter electrodes, it is not infrequent to read about electrochemical tests carried out using metal CEs in two-electrode setups and in a variety of electrolyte systems. While it is well known that Mg metal has considerable difficulties in achieving a stable, reproducible stripping/plating with low overpotential,^[198] little can be done with Ca metal, if not using specific electrolyte solutions and temperature conditions.^[12,13] In these cases, reporting electrochemical measurements in two-electrode setups, using metal CEs, can be misleading, due to strong influence of kinetic limitations from both the Working Electrode (WE) and the CE. A viable alternative can be found in using a 3-electrode setup with AC CEs, due to their capacitive working principle, which should not influence the WE. In theory, a large AC electrode will not interfere during potential sweep or cycling, but is worth pointing out though, that such kind of carbon might not be devoid of possible side reactions with surface groups^[199] and a careful balancing of the electrode should be conducted in order to avoid unwanted side reactions with the electrolyte.^[200]

The WE is the focal point of every electrochemical experiment since it is the side on the electrochemical cell in which the material or the process of interest is being investigated. From a reader's perspective, the WE side combines the hurdles of the CE and RE, with a correct interpretation of electrochemical and additional data. From this point of view, cell setup becomes another crucial parameter to be correctly chosen and implemented upon running the experiment. In these last few years, several review papers listed and commented on the most suitable and reliable cell setups to be used to evaluate electrochemical experiments.^[201]

The history of cell configuration used to assess a potential intercalation cathode for multivalent cations in non-aqueous electrolyte such as Mg and Ca shows up a questionable approach.^[42] It is found that, a three-electrode setup is required in order to efficiently monitor and conduct an experiment, especially in the field of MIBs, where fundamental science is involved, to fully understand the processes occurring at the very core of the material. In this view, for cycling experiments and potential-controlled experiments like CVs a simple three-electrode Swagelok-cell setup may be the easiest and most viable option, while for more sensitive interface-related experiments like PEIS, much more care needs to be applied, and setups with a better geometry and electrode placement could be found.^[202] In any case, until now, there is not an optimized or suitable cell-setup, which could be recommended with confidence to investigate the intercalation and extraction processes of Mg^{2+} and Ca^{2+} cations.

Finally, a search for an alternative "universal" reference electrode for Mg or Ca, in their respective chemistries, should be also listed as a priority task.

7. Summary And Outlook

Exploring new alternatives and viable energy storage technologies to meet the requirements of the increasingly energy-intensive applications is of paramount interest. Multivalent-ion batteries based on Mg and Ca chemistries could represent alternatives to the well-established LIBs. Nevertheless, this requires a careful and thorough development to establish reliable and reproducible research methods, which until now has been a considerable challenge.

The importance of insertion parameters affecting Mg^{2+} and Ca^{2+} diffusion has been taken into consideration. Understanding and developing different strategies to improve the sluggish intercalation of divalent cations compared to the monovalent cations such as Li^+ or Na^+ is of fundamental importance. These aspects must not be taken for granted, since many aspects of intercalation processes have not been fully elucidated yet. Moreover, a deeper understanding of the role played by the interfaces/interphase at both the anode and cathode side is still required.

It is clear that research on Mg^{2+} and Ca^{2+} insertion cathodes is still in its infancy. However, thanks to an increasing interest in RMBs, new materials are being explored and a growing number of related papers are being published in scientific literature. Despite this, starting from the classical materials like layered TiS_2 and V_2O_5 structures to new investigations on Ti_2S_4 spinel and oxyfluoride species, a clear winner and possible candidate for a high-energy prototype system, is yet to be found. In this respect, cathode materials showing high capacities and operating at high potentials needs to be developed. Once the fundamental properties of the materials will be elucidated, proof-of-concept full cells with high loading, high areal capacities ($>3 \text{ mAh/cm}^2$) and dense electrode will have to be demonstrated in order to make these new technologies racing against Li-ion batteries. To that aim, and despite some encouraging new results, the state of research on electrolytes that have high conductivities ($>10 \text{ mS/cm}$), wide electrochemical window, that show compatibility with the cathode and that allow highly efficient deposition and dissolution of the alkali earth metals is to be advanced.

We also hope that effective research could be even more supported by theoretical calculations, e.g. DFT in order to improve the screening process of potential cathode materials and thus boost the fundamental research in post-Li chemistry storage technologies.

Finally, emphasis has been placed on the critical perspective of experimental protocols and currently used approaches in post-Li storage research, since there are still major issues related to the investigation of anode/electrolyte/cathode systems, cell configurations and data reporting. Those aspects are crucial to prevent misinterpretation of results. We here note that still reports dealing with the electrochemical characterization of cathode materials in electrolytes that do not allow Mg/Ca plating/stripping and yet with the alkali earth metals used as counter and/or reference electrode, thus undermining the reliability of the reported results, can be found. In addition, since it is often difficult to implement in current multivalent

experimental practice, Ca- and Mg-metal QREs, and given the increasing popularity of alternative pseudo-reference and counter electrodes, systematic studies on their actual working mechanism and a common practice on calibration procedures, which should be reported every time, would be much beneficial to the community.

Acknowledgements

This work contributes to the research performed at CELEST (Center for Electrochemical Energy Storage Ulm-Karlsruhe) and was funded by the German Research Foundation (DFG) under Project ID 390874152 (POLIS Cluster of Excellence).

Conflict of Interest

The authors declare no conflict of interest.

Keywords: magnesium batteries • calcium batteries • cathode materials • multivalent batteries • energy storage

- [1] a) M. Aneke, M. Wang, *Appl. Energy* **2016**, *179*, 35; b) M. Marinaro, D. Bresser, E. Beyer, P. Faguy, K. Hosoi, H. Li, J. Sakovica, K. Amine, M. Wohlfahrt-Mehrens, S. Passerini, *J. Power Sources* **2020**, *459*, 22807
- [2] B. Di Pietro, M. Patriarca, B. Scrosati, *J. Power Sources* **1982**, *8*, 289.
- [3] M. V. Reddy, A. Mauger, C. M. Julien, A. Paoletta, K. Zaghib, *Materials* **2020**, *13*, 1884.
- [4] Y. Ding, Z. P. Cano, A. Yu, J. Lu, Z. Chen, *Electrochem. Energy Rev.* **2019**, *2*, 1.
- [5] R. Schmuck, R. Wagner, G. Hörpel, T. Placke, M. Winter, *Nat. Energy* **2018**, *3*, 267.
- [6] a) W. Lv, Z. Wang, H. Cao, Y. Sun, Y. Zhang, Z. Sun, *ACS Sustainable Chem. Eng.* **2018**, *6*, 1504; b) Velázquez-Martínez, Valio, Santasalo-Aarnio, Reuter, Serna-Guerrero, *Batteries* **2019**, *5*, 68.
- [7] L. Chen, M. Fiore, J. E. Wang, R. Ruffo, D.-K. Kim, G. Longoni, *Adv. Sustainable Syst.* **2018**, *2*, 1700153.
- [8] S. M. Selis, J. P. Wondowski, R. F. Justus, *J. Electrochem. Soc.* **1964**, *111*, 6.
- [9] L. W. Gaddum, H. E. French, *J. Am. Chem. Soc.* **1927**, *49*, 1295.
- [10] D. Aurbach, Z. Lu, A. Schechter, Y. Gofer, H. Gizbar, R. Turgeman, Y. Cohen, M. Moshkovich, E. Levi, *Nature* **2000**, *407*, 724.
- [11] L. Mei, J. Xu, Z. Wei, H. Liu, Y. Li, J. Ma, S. Dou, *Small* **2017**, *13*, 1701441.
- [12] D. Wang, X. Gao, Y. Chen, L. Jin, C. Kuss, P. G. Bruce, *Nat. Mater.* **2018**, *17*, 16.
- [13] A. Ponrouch, C. Frontera, F. Bardé, M. R. Palacín, *Nat. Mater.* **2016**, *15*, 169.
- [14] E. Peled, D. Golodntsky, G. Ardel, C. Menachem, D. Bar Tow, V. Eshkenazy, *MRS Proc.* **1995**, 393.
- [15] X.-B. Cheng, R. Zhang, C.-Z. Zhao, Q. Zhang, *Chem. Rev.* **2017**, *117*, 10403.
- [16] I. Hasa, S. Mariyappan, D. Sauré, P. Adelhelm, A. Y. Koposov, C. Masquelier, L. Croguennec, M. Casas-Cabanas, *J. Power Sources* **2021**, *482*, 228872.
- [17] P. K. Nayak, L. Yang, W. Brehm, P. Adelhelm, *Angew. Chem. Int. Ed.* **2018**, *57*, 102.
- [18] J. Muldoon, C. B. Bucur, T. Gregory, *Chem. Rev.* **2014**, *114*, 11683.
- [19] P. W. Atkins, D. F. Shriver, *Inorganic Chemistry*, Oxford University Press, Oxford, **2006**.
- [20] Y. Liang, H. D. Yoo, Y. Li, J. Shuai, H. A. Calderon, F. C. Robles Hernandez, L. C. Grabow, Y. Yao, *Nano Lett.* **2015**, *15*, 2194.
- [21] R. D. Shannon, *Acta Crystallogr. Sect. A* **1976**, *32*, 751.
- [22] T. D. Gregory, R. J. Hoffman, R. C. Winterton, *J. Electrochem. Soc.* **1990**, *137*, 775.
- [23] R. E. Doe, R. Han, J. Hwang, A. J. Gmitter, I. Shterenberg, H. D. Yoo, N. Pour, D. Aurbach, *Chem. Commun.* **2014**, *50*, 243.
- [24] a) C. Liao, N. Sa, B. Key, A. K. Burrell, L. Cheng, L. A. Curtiss, J. T. Vaughan, J.-J. Woo, L. Hu, B. Pan et al., *J. Mater. Chem. A* **2015**, *3*, 6082; b) L. C. Merrill, J. L. Schaefer, *Langmuir* **2017**, *33*, 9426; c) S. Dongmo, S. Zaibitzer, P. Schüler, S. Krieck, L. Jörissen, M. Wohlfahrt-Mehrens, M. Westerhausen, M. Marinaro, *ChemSusChem* **2020**, *13*, 3530.
- [25] T. J. Carter, R. Mohtadi, T. S. Arthur, F. Mizuno, R. Zhang, S. Shirai, J. W. Kampf, *Angew. Chem. Int. Ed.* **2014**, *53*, 3173.
- [26] R. Schwarz, M. Pejic, P. Fischer, M. Marinaro, L. Jörissen, M. Wachtler, *Angew. Chem.* **2016**, *128*, 15182.
- [27] D. Aurbach, R. Skaletsky, Y. Gofer, *J. Electrochem. Soc.* **1991**, *138*, 3536.
- [28] R. Attias, M. Salama, B. Hirsch, Y. Gofer, D. Aurbach, *Joule* **2019**, *3*, 27.
- [29] Q. Guo, W. Zeng, S.-L. Liu, Y.-Q. Li, J.-Y. Xu, J.-X. Wang, Y. Wang, *Rare Met.* **2020**, *8*, 1702582.
- [30] A. Shyamsunder, L. E. Blanc, A. Assoud, L. F. Nazar, *ACS Energy Lett.* **2019**, *4*, 2271.
- [31] Z. Li, O. Fuhr, M. Fichtner, Z. Zhao-Karger, *Energy Environ. Sci.* **2019**, *12*, 3496.
- [32] A. Ponrouch, D. Tchitchevka, C. Frontera, F. Bardé, M. A.-d. Domípablo, M. R. Palacín, *Electrochim. Commun.* **2016**, *66*, 75.
- [33] A. Jain, Y. Shin, K. A. Persson, *Nat. Rev. Mater.* **2016**, *1*, 714.
- [34] D. S. Tchitchevka, A. Ponrouch, R. Verrelli, T. Broux, C. Frontera, A. Sorrentino, F. Bardé, N. Biskup, M. E. Arroyo-de Domípablo, M. R. Palacín, *Chem. Mater.* **2018**, *30*, 847.
- [35] A. Parija, D. Prendergast, S. Banerjee, *ACS Appl. Mater. Interfaces* **2017**, *9*, 23756.
- [36] T. R. Juran, J. Young, M. Smeu, *J. Phys. Chem. C* **2018**, *122*, 8788.
- [37] M. Liu, Z. Rong, R. Malik, P. Canepa, A. Jain, G. Ceder, K. A. Persson, *Energy Environ. Sci.* **2015**, *8*, 964.
- [38] M. E. Arroyo-de Domípablo, C. Krich, J. Nava-Avendaño, M. R. Palacín, F. Bardé, *Phys. Chem. Chem. Phys.* **2016**, *18*, 19966.
- [39] M. Smeu, M. S. Hossain, Z. Wang, V. Timoshevskii, K. H. Bevan, K. Zaghib, *J. Power Sources* **2016**, *306*, 431.
- [40] A. L. Lipson, S.-D. Han, S. Kim, B. Pan, N. Sa, C. Liao, T. T. Fister, A. K. Burrell, J. T. Vaughan, B. J. Ingram, *J. Power Sources* **2016**, *325*, 646.
- [41] F. Liu, T. Wang, X. Liu, L.-Z. Fan, *Adv. Energy Mater.* **2020**, *36*, 2000787.
- [42] P. Canepa, G. Sai Gautam, D. C. Hannah, R. Malik, M. Liu, K. G. Gallagher, K. A. Persson, G. Ceder, *Chem. Rev.* **2017**, *117*, 4287.
- [43] M. E. Arroyo-de Domípablo, A. Ponrouch, P. Johansson, M. R. Palacín, *Chem. Rev.* **2019**, *120*, 6331.
- [44] L. Li, Y. Lu, Q. Zhang, S. Zhao, Z. Hu, S.-L. Chou, *Small* **2019**, *15*, 1902767.
- [45] D. Aurbach, G. S. Suresh, E. Levi, A. Mitelman, O. Mizrahi, O. Chusid, M. Brunelli, *Adv. Mater.* **2007**, *19*, 4260.
- [46] Z. Zhao-Karger, M. E. Gil Bardaji, O. Fuhr, M. Fichtner, *J. Mater. Chem. A* **2017**, *5*, 10815.
- [47] O. Tutusaus, R. Mohtadi, T. S. Arthur, F. Mizuno, E. G. Nelson, Y. V. Sevryugina, *Angew. Chem. Int. Ed.* **2015**, *54*, 7900.
- [48] X. Sun, L. Blanc, G. M. Nolis, P. Bonnick, J. Cabana, L. F. Nazar, *Chem. Mater.* **2018**, *30*, 121.
- [49] Z. Li, X. Mu, Z. Zhao-Karger, T. Diemant, R. J. Behm, C. Kübel, M. Fichtner, *Nat. Commun.* **2018**, *9*, 5115.
- [50] J. Luo, Y. Bi, L. Zhang, X. Zhang, T. L. Liu, *Angew. Chem. Int. Ed.* **2019**, *58*, 6967.
- [51] J. T. Incorvati, L. F. Wan, B. Key, D. Zhou, C. Liao, L. Fuoco, M. Holland, H. Wang, D. Prendergast, K. R. Poeppelmeier et al., *Chem. Mater.* **2016**, *28*, 17.
- [52] Q. An, Y. Li, H. Deog Yoo, S. Chen, Q. Ru, L. Mai, Y. Yao, *Nano Energy* **2015**, *18*, 265.
- [53] M. Bervas, L. C. Klein, G. G. Amatucci, *Solid State Ionics* **2005**, *176*, 2735.
- [54] H. Tang, F. Xiong, Y. Jiang, C. Pei, S. Tan, W. Yang, M. Li, Q. An, L. Mai, *Nano Energy* **2019**, *58*, 347.
- [55] E. A. Esparcia, M. S. Chae, J. D. Ocon, S.-T. Hong, *Chem. Mater.* **2018**, *30*, 3690.
- [56] G. Gershinsky, H. D. Yoo, Y. Gofer, D. Aurbach, *Langmuir* **2013**, *29*, 10964.
- [57] M. Cabello, F. Nacimiento, R. Alcántara, P. Lavela, C. Pérez Vicente, J. L. Tirado, *Chem. Mater.* **2018**, *30*, 5853.
- [58] Z.-L. Tao, L.-N. Xu, X.-L. Gou, J. Chen, H.-T. Yuan, *Chem. Commun.* **2004**, *2080*.
- [59] X. Ji, J. Chen, F. Wang, W. Sun, Y. Ruan, L. Miao, J. Jiang, C. Wang, *Nano Lett.* **2018**, *18*, 6441.
- [60] Y. Orikasa, T. Masese, Y. Koyama, T. Mori, M. Hattori, K. Yamamoto, T. Okado, Z.-D. Huang, T. Minato, C. Tassel et al., *Sci. Rep.* **2014**, *4*, 5622.

- [61] K. Makino, Y. Katayama, T. Miura, T. Kishi, *J. Power Sources* **2001**, *99*, 66.
- [62] S. Kim, L. Yin, M. H. Lee, P. Parajuli, L. Blanc, T. T. Fister, H. Park, B. J. Kwon, B. J. Ingram, P. Zapol et al., *ACS Energy Lett.* **2020**, *5*, 3203.
- [63] Q. D. Truong, M. Kempaiah Devaraju, P. D. Tran, Y. Gambe, K. Nayuki, Y. Sasaki, I. Honma, *Chem. Mater.* **2017**, *29*, 6245.
- [64] T. Ichitsubo, T. Adachi, S. Yagi, T. Doi, *J. Mater. Chem.* **2011**, *21*, 11764.
- [65] M. Cabello, R. Alcántara, F. Nacimiento, G. Ortiz, P. Lavela, J. L. Tirado, *CrystEngComm* **2015**, *17*, 8728.
- [66] M. Cabello, F. Nacimiento, J. R. González, G. Ortiz, R. Alcántara, P. Lavela, C. Pérez-Vicente, J. L. Tirado, *Electrochim. Commun.* **2016**, *67*, 59.
- [67] T. Tojo, Y. Sugiura, R. Inada, Y. Sakurai, *Electrochim. Acta* **2016**, *207*, 22.
- [68] A. L. Lipson, B. Pan, S. H. Lapidus, C. Liao, J. T. Vaughney, B. J. Ingram, *Chem. Mater.* **2015**, *27*, 8442.
- [69] A. L. Lipson, S. Kim, B. Pan, C. Liao, T. T. Fister, B. J. Ingram, *J. Power Sources* **2017**, *369*, 133.
- [70] L. Stievano, I. de Meata, J. Bitenc, C. Cavallo, S. Brutt, M. A. Navarra, *J. Power Sources* **2021**, *482*, 228875.
- [71] R. E. Doe, T. K. Mueller, G. Ceder, J. Barker, K. A. Persson, US 9077032 B2, 2012.
- [72] R. Attias, M. Salama, B. Hirsch, Y. Gofer, D. Aurbach, *ChemElectroChem* **2018**, *5*, 3514.
- [73] a) A. Chakraborty, S. Kunnikuruvan, S. Kumar, B. Markovsky, D. Aurbach, M. Dixit, D. T. Major, *Chem. Mater.* **2020**, *32*, 915; b) Y. Zhao, P. Stein, Y. Bai, M. Al-Siraj, Y. Yang, B.-X. Xu, *J. Power Sources* **2019**, *413*, 259; c) K. Tasaki, K. Kanda, T. Kobayashi, S. Nakamura, M. Ue, *Electrochim. Acta* **2006**, *153*, A2192.
- [74] a) S. Choudhury, S. Wei, Y. Ozhabes, D. Gunceler, M. J. Zachman, Z. Tu, J. H. Shin, P. Nath, A. Agrawal, L. F. Kourkoutis et al., *Nat. Commun.* **2017**, *8*, 898; b) E. Watanabe, S.-C. Chung, S.-i. Nishimura, Y. Yamada, M. Okubo, K. Sodeyama, Y. Tateyama, A. Yamada, *Chem. Rec.* **2019**.
- [75] E. Levi, M. D. Levi, O. Chasid, D. Aurbach, *J. Electroceram.* **2009**, *22*, 13.
- [76] H. C. Herbol, J. Stevenson, P. Clancy, *J. Chem. Theory Comput.* **2017**, *13*, 3250.
- [77] Z. Rong, R. Malik, P. Canepa, G. Sai Gautam, M. Liu, A. Jain, K. Persson, G. Ceder, *Chem. Mater.* **2015**, *27*, 6016.
- [78] M. Mao, X. Ji, S. Hou, T. Gao, F. Wang, L. Chen, X. Fan, J. Chen, J. Ma, C. Wang, *Chem. Mater.* **2019**, *31*, 3183.
- [79] Y. Zhang, H. Geng, W. Wei, J. Ma, L. Chen, C. C. Li, *Energy Storage Mater.* **2019**, *20*, 118.
- [80] C. M. MacLaughlin, *ACS Energy Lett.* **2019**, *4*, 572.
- [81] J. Muldoon, C. B. Bucur, T. Gregory, *Angew. Chem. Int. Ed.* **2017**, *56*, 12064.
- [82] X. Sun, P. Bonnick, L. F. Nazar, *ACS Energy Lett.* **2016**, *1*, 297.
- [83] R. Chen, R. Luo, Y. Huang, F. Wu, L. Li, *Adv. Sci.* **2016**, *3*, 1600051.
- [84] M. K. Aydinol, A. F. Kohan, G. Ceder, K. Cho, J. Joannopoulos, *Phys. Rev. B* **1997**, *56*, 1354.
- [85] P. Novák, R. Imhof, O. Haas, *Electrochim. Acta* **1999**, *45*, 351.
- [86] E. Levi, Y. Gofer, D. Aurbach, *Chem. Mater.* **2010**, *22*, 860.
- [87] a) S. Terada, T. Mandai, S. Suzuki, S. Tsuzuki, K. Watanabe, Y. Kamei, K. Ueno, K. Dokko, M. Watanabe, *J. Phys. Chem. C* **2016**, *120*, 1353; b) J. P. Pereira-Ramos, R. Messina, J. Perichon, *J. Electroanal. Chem. Interfacial Electrochem.* **1987**, *218*, 241.
- [88] P. Novák, *J. Electrochem. Soc.* **1993**, *140*, 140.
- [89] K. Zhang, G. Gao, W. Sun, X. Liang, Y. Liu, G. Wu, *RSC Adv.* **2018**, *8*, 22053.
- [90] G. Sai Gautam, P. Canepa, A. Abdellahi, A. Urban, R. Malik, G. Ceder, *Chem. Mater.* **2015**, *27*, 3733.
- [91] P. Millet, C. Satto, P. Sciau, J. Galy, *J. Solid State Chem.* **1998**, *136*, 56.
- [92] B. Zhou, H. Shi, R. Cao, X. Zhang, Z. Jiang, *Phys. Chem. Chem. Phys.* **2014**, *16*, 18578.
- [93] R. Xiao, J. Xie, T. Luo, L. Huang, Y. Zhou, D. Yu, C. Chen, Y. Liu, *J. Phys. Chem. C* **2018**, *122*, 1513.
- [94] D. Imamura, M. Miyayama, M. Hibino, T. Kudo, *J. Electrochem. Soc.* **2003**, *150*, A753.
- [95] D. Imamura, M. Miyayama, *Solid State Ionics* **2003**, *161*, 173.
- [96] S. H. Lee, R. A. DiLeo, A. C. Marschilok, K. J. Takeuchi, E. S. Takeuchi, *ECS Electrochem. Lett.* **2014**, *3*, A87-A90.
- [97] G. Sai Gautam, P. Canepa, W. D. Richards, R. Malik, G. Ceder, *Nano Lett.* **2016**, *16*, 2426.
- [98] S. D. Perera, R. B. Archer, C. A. Damin, R. Mendoza-Cruz, C. P. Rhodes, *J. Power Sources* **2017**, *343*, 580.
- [99] X. Du, G. Huang, Y. Qin, L. Wang, *RSC Adv.* **2015**, *5*, 76352.
- [100] K. W. Nam, S. Kim, S. Lee, M. Salama, I. Shterenberg, Y. Gofer, J.-S. Kim, E. Yang, C. S. Park, J.-S. Kim et al., *Nano Lett.* **2015**, *15*, 4071.
- [101] a) T. S. Arthur, R. Zhang, C. Ling, P.-A. Glans, X. Fan, J. Guo, F. Mizuno, *ACS Appl. Mater. Interfaces* **2014**, *6*, 7004; b) R. Zhang, X. Yu, K.-W. Nam, C. Ling, T. S. Arthur, W. Song, A. M. Knapp, S. N. Ehrlich, X.-Q. Yang, M. Matsui, *Electrochim. Commun.* **2012**, *23*, 110; c) R. Zhang, T. S. Arthur, C. Ling, F. Mizuno, *J. Power Sources* **2015**, *282*, 630; d) C. Ling, R. Zhang, T. S. Arthur, F. Mizuno, *Chem. Mater.* **2015**, *27*, 5799.
- [102] X. Sun, V. Duffort, B. L. Mehdi, N. D. Browning, L. F. Nazar, *Chem. Mater.* **2016**, *28*, 534.
- [103] C. Kim, P. J. Phillips, B. Key, T. Yi, D. Nordlund, Y.-S. Yu, R. D. Bayliss, S.-D. Han, M. He, Z. Zhang et al., *Adv. Mater.* **2015**, *27*, 3377.
- [104] J. Reed, G. Ceder, A. van der Ven, *Electrochim. Solid-State Lett.* **2001**, *4*, A78.
- [105] M. E. Spahr, P. Novák, O. Haas, R. Nesper, *J. Power Sources* **1995**, *54*, 346.
- [106] L. F. Wan, J. T. Incorvati, K. R. Poepelmeier, D. Prendergast, *Chem. Mater.* **2016**, *28*, 6900.
- [107] a) T. S. Sian, G. B. Reddy, S. M. Shivaprasad, *Electrochim. Solid-State Lett.* **2006**, *9*, A120; b) T. S. Sian, G. B. Reddy, S. M. Shivaprasad, *Jpn. J. Appl. Phys.* **2004**, *43*, 6248.
- [108] W. Kaveevivitchai, A. J. Jacobson, *Chem. Mater.* **2016**, *28*, 4593.
- [109] W. Kaveevivitchai, A. J. Jacobson, *Chem. Mater.* **2013**, *25*, 2708.
- [110] M. Mao, T. Gao, S. Hou, C. Wang, *Chem. Soc. Rev.* **2018**, *47*, 8804.
- [111] N. Amir, Y. Vestfrid, O. Chusid, Y. Gofer, D. Aurbach, *J. Power Sources* **2007**, *174*, 1234.
- [112] A. Emly, A. van der Ven, *Inorg. Chem.* **2015**, *54*, 4394.
- [113] H. D. Yoo, Y. Liang, H. Dong, J. Lin, H. Wang, Y. Liu, L. Ma, T. Wu, Y. Li, Q. Ru et al., *Nat. Commun.* **2017**, *8*, 339.
- [114] S. Yang, D. Li, T. Zhang, Z. Tao, J. Chen, *J. Phys. Chem. C* **2012**, *116*, 1307.
- [115] X.-L. Li, Y.-D. Li, *J. Phys. Chem. B* **2004**, *108*, 13893.
- [116] Y. Liang, R. Feng, S. Yang, H. Ma, J. Liang, J. Chen, *Adv. Mater.* **2011**, *23*, 640.
- [117] Z. Li, B. P. Vinayan, P. Jankowski, C. Njel, A. Roy, T. Vegge, J. Maibach, J. M. G. Lastra, M. Fichtner, Z. Zhao-Karger, *Angew. Chem. Int. Ed.* **2020**, *59*, 11483.
- [118] Y. Wang, Z. Liu, C. Wang, X. Yi, R. Chen, L. Ma, Y. Hu, G. Zhu, T. Chen, Z. Tie et al., *Adv. Mater.* **2018**, *30*, e1802563.
- [119] a) M. Naguib, M. Kurtoglu, V. Presser, J. Lu, J. Niu, M. Heon, L. Hultman, Y. Gogotsi, M. W. Barsoum, *Adv. Mater.* **2011**, *23*, 4248; b) C. Eames, M. S. Islam, *J. Am. Chem. Soc.* **2014**, *136*, 16270.
- [120] M. Rashad, M. Asif, Y. Wang, Z. He, I. Ahmed, *Energy Storage Mater.* **2020**, *25*, 342.
- [121] M. Xu, S. Lei, J. Qi, Q. Dou, L. Liu, Y. Lu, Q. Huang, S. Shi, X. Yan, *ACS Nano* **2018**, *12*, 3733.
- [122] F. Liu, Y. Liu, X. Zhao, X. Liu, L.-Z. Fan, *J. Mater. Chem. A* **2019**, *7*, 16712.
- [123] M.-Q. Zhao, C. E. Ren, M. Alhabeb, B. Anasori, M. W. Barsoum, Y. Gogotsi, *ACS Appl. Energy Mater.* **2019**, *2*, 1572.
- [124] A. Byeon, M.-Q. Zhao, C. E. Ren, J. Halim, S. Kota, P. Urbankowski, B. Anasori, M. W. Barsoum, Y. Gogotsi, *ACS Appl. Mater. Interfaces* **2017**, *9*, 4296.
- [125] X. Duan, J. Xu, Z. Wei, J. Ma, S. Guo, H. Liu, S. Dou, *Small Methods* **2017**, *1*, 1700156.
- [126] Y. Gu, Y. Katsura, T. Yoshino, H. Takagi, K. Taniguchi, *Sci. Rep.* **2015**, *5*, 12486.
- [127] B. Liu, T. Luo, G. Mu, X. Wang, Di Chen, G. Shen, *ACS Nano* **2013**, *7*, 8051.
- [128] L. Zhou, Q. Liu, Z. Zhang, K. Zhang, F. Xiong, S. Tan, Q. An, Y.-M. Kang, Z. Zhou, L. Mai, *Adv. Mater.* **2018**, *30*, e1801984.
- [129] C. Masquelier, L. Croguennec, *Chem. Rev.* **2013**, *113*, 6552.
- [130] A. Manthiram, *Nat. Commun.* **2020**, *11*, 1550.
- [131] T. Jin, H. Li, K. Zhu, P.-F. Wang, P. Liu, L. Jiao, *Chem. Soc. Rev.* **2020**, *49*, 2342.
- [132] Z. Gong, Y. Yang, *Energy Environ. Sci.* **2011**, *4*, 3223.
- [133] C. Julien, A. Mauger, A. Vijh, K. Zaghib in *Lithium Batteries* (Eds.: C. Julien, A. Mauger, A. Vijh, K. Zaghib), Springer International Publishing, Cham, **2016**, pp. 201–268.
- [134] C. Ling, D. Banerjee, W. Song, M. Zhang, M. Matsui, *J. Mater. Chem.* **2012**, *22*, 13517.
- [135] T. Mori, T. Masese, Y. Oriksa, Z.-D. Huang, T. Okado, J. Kim, Y. Uchimoto, *Phys. Chem. Chem. Phys.* **2016**, *18*, 13524.
- [136] S. A. T. Redfern, C. M. B. Henderson, B. J. Wood, R. J. Harrison, K. S. Knight, *Nature* **1996**, *381*, 407.
- [137] J. Heath, H. Chen, M. S. Islam, *J. Mater. Chem. A* **2017**, *5*, 13161.

- [138] Z. Feng, J. Yang, Y. NuLi, J. Wang, X. Wang, Z. Wang, *Electrochim. Commun.* **2008**, *10*, 1291.
- [139] Z. Feng, J. Yang, Y. NuLi, J. Wang, *J. Power Sources* **2008**, *184*, 604.
- [140] Y. NuLi, J. Yang, Y. Li, J. Wang, *Chem. Commun.* **2010**, *46*, 3794.
- [141] Y. NuLi, J. Yang, J. Wang, Y. Li, *J. Phys. Chem. C* **2009**, *113*, 12594.
- [142] a) Y. Zheng, Y. NuLi, Q. Chen, Y. Wang, J. Yang, J. Wang, *Electrochim. Acta* **2012**, *66*, 75; b) Y. NuLi, Y. Zheng, Y. Wang, J. Yang, J. Wang, *J. Mater. Chem.* **2011**, *21*, 12437.
- [143] Q. D. Truong, M. K. Devaraju, I. Honma, *J. Power Sources* **2017**, *361*, 195.
- [144] A. K. Padhi, *J. Electrochem. Soc.* **1997**, *144*, 1188.
- [145] N. Ravel, J. B. Goodenough, S. Besner, M. Simoneau, P. Hovington, M. Armand, "Improved iron based cathode material". Extended Abstract of The Electrochemical Society Meeting **1999**.
- [146] a) M. Zhang, N. Garcia-Araez, A. L. Hector, *J. Mater. Chem. A* **2018**, *6*, 14483; b) A. Osnis, M. Kosa, D. Aurbach, D. T. Major, *J. Phys. Chem. C* **2013**, *117*, 17919; c) J. Li, S. Luo, X. Ding, Q. Wang, P. He, *ACS Appl. Mater. Interfaces* **2018**, *10*, 10786.
- [147] Y. Fang, J. Zhang, L. Xiao, X. Ai, Y. Cao, H. Yang, *Adv. Sci.* **2017**, *4*, 1600392.
- [148] R. Zhang, C. Ling, *ACS Appl. Mater. Interfaces* **2016**, *8*, 18018.
- [149] K. Makino, Y. Katayama, T. Miura, T. Kishi, *J. Power Sources* **2001**, *97*-98, 512.
- [150] Z.-D. Huang, T. Masese, Y. Orikasa, T. Mori, k. Yamamoto, *RSC Adv.* **2015**, *5*, 8598.
- [151] J. Zeng, Y. Yang, S. Lai, J. Huang, Y. Zhang, J. Wang, J. Zhao, *Chem. Eur. J.* **2017**, *23*, 16898.
- [152] Y.-U. Park, D.-H. Seo, B. Kim, K.-P. Hong, H. Kim, S. Lee, R. A. Shakoor, K. Miyasaka, J.-M. Tarascon, K. Kang, *Sci. Rep.* **2012**, *2*, 704.
- [153] Z.-D. Huang, T. Masese, Y. Orikasa, T. Mori, T. Minato, C. Tassel, Y. Kobayashi, H. Kageyama, Y. Uchimoto, *J. Mater. Chem. A* **2014**, *2*, 11578.
- [154] W. Jin, G. Yin, Z. Wang, Y. Q. Fu, *Appl. Surf. Sci.* **2016**, *385*, 72.
- [155] D. Aurbach, I. Weissman, Y. Gofer, E. Levi, *Chem. Rec.* **2003**, *3*, 61.
- [156] R. Mohtadi, M. Matsui, T. S. Arthur, S.-J. Hwang, *Angew. Chem. Int. Ed.* **2012**, *51*, 9780.
- [157] Hiroo Kawaia, Mikito Nagatab, Hiroyuki Kageyamac, Hisashi Tukamotob, *Electrochim. Acta* **1999**, *315*.
- [158] C. Yuan, Y. Zhang, Y. Pan, X. Liu, G. Wang, D. Cao, *Electrochim. Acta* **2014**, *116*, 404.
- [159] M. Liu, A. Jain, Z. Rong, X. Qu, P. Canepa, R. Malik, G. Ceder, K. A. Persson, *Energy Environ. Sci.* **2016**, *9*, 3201.
- [160] J. C. Knight, S. Therese, A. Manthiram, *ACS Appl. Mater. Interfaces* **2015**, *7*, 22953.
- [161] C. Kim, A. A. Adil, R. D. Bayliss, T. L. Kinnibrugh, S. H. Lapidus, G. M. Nolis, J. W. Freeland, P. J. Phillips, T. Yi, H. D. Yoo et al., *Chem. Mater.* **2018**, *30*, 1496.
- [162] Z. Feng, X. Chen, L. Qiao, A. L. Lipson, T. T. Fister, L. Zeng, C. Kim, T. Yi, N. Sa, D. L. Proffit et al., *ACS Appl. Mater. Interfaces* **2015**, *7*, 28438.
- [163] P. Canepa, S. Jayaraman, L. Cheng, N. N. Rajput, W. D. Richards, G. S. Gautam, L. A. Curtiss, K. A. Persson, G. Ceder, *Energy Environ. Sci.* **2015**, *8*, 3718.
- [164] J. Yin, A. B. Brady, E. S. Takeuchi, A. C. Marschilok, K. J. Takeuchi, *Chem. Commun.* **2017**, *53*, 3665.
- [165] A. Emly, A. van der Ven, *Inorg. Chem.* **2015**, *54*, 4394.
- [166] Y. Tashiro, K. Taniguchi, H. Miyasaka, *Electrochim. Acta* **2016**, *210*, 655.
- [167] X. Sun, P. Bonnick, L. F. Nazar, *ACS Energy Lett.* **2016**, *1*, 297.
- [168] X. Sun, P. Bonnick, V. Duffort, M. Liu, Z. Rong, K. A. Persson, G. Ceder, L. F. Nazar, *Energy Environ. Sci.* **2016**, *9*, 2273.
- [169] V. V. Kulish, D. Koch, S. Manzhos, *Phys. Chem. Chem. Phys.* **2017**, *19*, 6076.
- [170] P. Canepa, S.-H. Bo, G. Sai Gautam, B. Key, W. D. Richards, T. Shi, Y. Tian, Y. Wang, J. Li, G. Ceder, *Nat. Commun.* **2017**, *8*, 1759.
- [171] J. Koettgen, C. J. Bartel, G. Ceder, *Chem. Commun.* **2020**, *56*, 1952.
- [172] D. C. Hannah, G. Sai Gautam, P. Canepa, Z. Rong, G. Ceder, *Chem. Commun.* **2017**, *53*, 5171.
- [173] R. D. Shannon, C. T. Prewitt, *Acta Crystallogr. Sect. B* **1969**, *25*, 925.
- [174] S.-M. Chen, *J. Electroanal. Chem.* **2002**, *521*, 29.
- [175] M. Hayashi, H. Arai, H. Ohtsuka, Y. Sakurai, *Electrochim. Solid-State Lett.* **2004**, *7*, A119.
- [176] P. Padigi, G. Goncher, D. Evans, R. Solanki, *J. Power Sources* **2015**, *273*, 460.
- [177] A. Torres, F. J. Luque, J. Tortajada, M. E. Arroyo-de Dompablo, *Sci. Rep.* **2019**, *9*, 9644.
- [178] D. Wang, H. Liu, J. D. Elliott, L.-M. Liu, W.-M. Lau, *J. Mater. Chem. A* **2016**, *4*, 12516.
- [179] M. E. A.-d. Dompablo, C. Krich, J. Nava-Avendaño, N. Biškup, M. R. Palacín, F. Bardé, *Chem. Mater.* **2016**, *28*, 6886.
- [180] G. Jouravsky, F. Permingeat, C. Gaudefroy, *Bulletin de Minéralogie* **1963**, *359*.
- [181] L. Folco, M. Mellini, *Eur. J. Mineral.* **1997**, *9*, 969.
- [182] a) R. G. Burns, *Orthosilicates*, De Gruyter, Berlin, Boston, **1982**; b) D. Morgan, A. van der Ven, G. Ceder, *Electrochim. Solid-State Lett.* **2004**, *7*, A30.
- [183] A. Varela, S. d. Dios, M. Parras, M. Hernando, M. T. Fernández-Díaz, A. R. Landa-Cánovas, J. M. González-Calbet, *J. Am. Chem. Soc.* **2009**, *131*, 8660.
- [184] Y. Miyazaki, X. Huang, T. Kajiwara, H. Yamane, T. Kajitani, *J. Ceram. Soc. Jpn.* **2009**, *117*, 42.
- [185] a) M. S. Whittingham, *Prog. Solid State Chem.* **1978**, *12*, 41; b) D. W. Murphy, F. J. Di Salvo, G. W. Hull, J. V. Waszczak, *Inorg. Chem.* **1976**, *15*, 17; c) C. M. Julien, *Mater. Sci. Eng. R.* **2003**, *40*, 47; d) R. Verrelli, A. P. Black, C. Pattanathummasid, D. S. Tchitchekova, A. Ponrouch, J. Oro-Solé, C. Frontera, F. Bardé, P. Rozier, M. R. Palacín, *J. Power Sources* **2018**, *407*, 162; e) Y. Murata, S. Takada, T. Obata, T. Tojo, R. Inada, Y. Sakurai, *Electrochim. Acta* **2019**, *294*, 210.
- [186] G. G. Amatucci, F. Badway, A. Singhal, B. Beaudoin, G. Skandan, T. Bowmer, I. Plitz, N. Pereira, T. Chapman, R. Jaworski, *J. Electrochem. Soc.* **2001**, *148*, A940.
- [187] a) C. Delmas, H. Cognac-Auradou, J. M. Coccantelli, M. Ménétrier, J. P. Doumerc, *Solid State Ionics* **1994**, *69*, 257; b) C. Zhang, Z. Chen, Z. Guo, X. W. Lou, *Energy Environ. Sci.* **2013**, *6*, 974.
- [188] C. Lee, Y.-T. Jeong, P. M. Nogales, H.-Y. Song, Y. Kim, R.-Z. Yin, S.-K. Jeong, *Electrochim. Commun.* **2019**, *98*, 115.
- [189] M. D. Radin, A. van der Ven, *Chem. Mater.* **2016**, *28*, 7898.
- [190] a) Prasanna Padigi, Neal Kuperman, J. Thiebes, G. Goncher, D. Evans, R. Solanki, *J. New Mater. Electrochim. Syst.* **2016**, *19*, 57; b) R. Y. Wang, C. D. Wessells, R. A. Huggins, Y. Cui, *Nano Lett.* **2013**, *13*, 5748.
- [191] C. Ling, D. Banerjee, W. Song, M. Zhang, M. Matsui, *J. Mater. Chem.* **2012**, *22*, 13517.
- [192] C. Ling, J. Chen, F. Mizuno, *J. Phys. Chem. C* **2013**, *117*, 21158.
- [193] Z. Gong, Y. Yang, *Energy Environ. Sci.* **2011**, *4*, 3223.
- [194] a) K. Izutsu, *Electrochemistry in Nonaqueous Solutions*, Wiley-VCH Verlag GmbH & Co. KGaA, Weinheim, FRG, **2002**; b) P. K. R. Kottam, S. Dongmo, M. Wohlfahrt-Mehrens, M. Marinaro, *Energies* **2020**, *13*, 1470.
- [195] P. K. R. Kottam, D. Kalkan, M. Wohlfahrt-Mehrens, M. Marinaro, *J. Electrochim. Soc.* **2019**, *166*, A1574-A1579.
- [196] R. Dugas, J. D. Forero-Saboya, A. Ponrouch, *Chem. Mater.* **2019**, *31*, 8613.
- [197] a) P. W. Ruch, D. Cericola, M. Hahn, R. Kötz, A. Wokaun, *J. Electroanal. Chem.* **2009**, *636*, 128; b) X. Liu, G. A. Elia, S. Passerini, *J. Power Sources Advances* **2020**, *2*, 100008.
- [198] R. Deivanayagam, B. J. Ingram, R. Shahbazian-Yassar, *Energy Storage Mater.* **2019**, *21*, 136.
- [199] K. Pfeifer, S. Arnold, J. Becherer, C. Das, J. Maibach, H. Ehrenberg, S. Dsoke, *ChemSusChem* **2019**, *12*, 3312.
- [200] A. Ponrouch, M. R. Palacín, *Curr. Opin. Electrochem.* **2018**, *9*, 1.
- [201] R. Nölle, K. Beltrop, F. Holtstiege, J. Kasnatscheew, T. Placke, M. Winter, *Mater. Today* **2020**, *32*, 131.
- [202] R. Raccichini, M. Amores, G. Hinds, *Batteries* **2019**, *5*, 12

Manuscript received: December 22, 2020

Revised manuscript received: February 11, 2021

Accepted manuscript online: February 23, 2021

Version of record online: April 20, 2021